RESEARCH ARTICLE SUMMARY

DEVELOPMENTAL SIGNALING

A molecular mechanism for Wnt ligand-specific signaling

Marie Eubelen*, Naguissa Bostaille*, Pauline Cabochette, Anne Gauquier, Patricia Tebabi, Andra C. Dumitru, Melanie Koehler, Philipp Gut, David Alsteens, Didier Y. R. Stainier, Abel Garcia-Pino, Benoit Vanhollebeke†

INTRODUCTION: Wnt signaling is an ancient signaling pathway that has accompanied the emergence of metazoans and is key to many developmental, physiological, and disease processes. Similar to other signaling pathways, gene families for both Wnt ligand and its corresponding Frizzled receptor have undergone extensive expansion during metazoan evolution. Vertebrate genomes harbor 19 closely related Wnt genes as well as 10 Frizzled genes. Gene duplication is typically considered a major driving force in the evolution of new biological functions through neo- or subfunctionalization of emerging paralogs. How this functional diversification of Wnt ligands is structurally and molecularly organized, however, remains poorly understood. The Wnt/Frizzled molecular interaction is mediated by residues conserved across both families. This promiscuous interaction is incompatible with monospecific recognition and, accordingly, when tested in pair-wise combinations, multiple Wnt ligands compete for binding to various Frizzled receptors.

RATIONALE: These observations raise the questions of how Wnt ligands achieve functional diversification and how cells interpret the intermingled expression patterns of simultaneous and sometimes conflicting Wnt signals. In some biological settings, cells may integrate all signaling inputs nondiscriminately and trigger appropriate responses by considering their total net balance. However, other biological processes exhibit strict Wnt ligand selectivity, despite complex Wnt/Frizzled expression landscapes. A prototypical example is provided by the exclusive control of mammalian forebrain and ventral spinal cord angiogenesis by Wnt7a and Wnt7b.

Within this neurovascular unit, in order to respond to neural progenitor–derived Wnt7 by activating Wnt/β-catenin signaling, cerebral endothelial cells must express a membrane protein complex consisting of the adhesion G protein–coupled receptor (GPCR) Gpr124 and the glycosylphosphatidylinositol-anchored glycoprotein Reck. This Gpr124/Reck complex was recently reported to promote Wnt7-specific responses.

RESULTS: Using a combination of biophysical approaches and ligand-binding assays in genetically engineered cells, we demonstrate that ligand selectivity is conferred by Reck, which mediates Wnt7-specific binding in a Frizzled-independent manner. Reck orchestrates Wnt ligand discrimination by engaging the structurally disordered and highly divergent linker domain of Wnt7. The presence of Gpr124 is required to deliver Reck-bound Wnt7 to Frizzled by assembling higher-order Reck/Gpr124/Frizzled/Lrp5/6 complexes. This Gpr124 tethering function does not rely on its GPCR structure but instead on its combined capacity to interact with Reck extracellularly and recruit the Dishevelled scaffolding protein intracellularly. By bridging Gpr124 and Frizzled, Dishevelled recruits Wnt7, via its association with Reck, into dynamic Wnt/Frizzled signalosomes, resulting in increased local concentrations of ligand available for Frizzled signaling.

ON OUR WEBSITE

Read the full article at http://dx.doi.org/10.1126/science.aat1178

CONCLUSION: Our data reveal that cells are equipped with "Wnt-decoding modules" that distinguish between Wnt ligands that are otherwise very similar. They also reveal a critical role for the linker domain in Wnt ligand evolution and functional diversification. These mechanistic insights into the Wnt decoding capacities of vertebrate cells predict that additional Wnt decoding modules exist, enabling fine-tuning of cellular behaviors in response to other Wnt or Frizzled family members. These modules expand the diversity of proximal events in Wnt signaling, opening new therapeutic opportunities for conditions in which Wnt stimulation or inhibition are desirable at the membrane level. In particular, the mechanisms uncovered here provide an opportunity for the targeted treatment of human central nervous system neurovascular disorders. ■

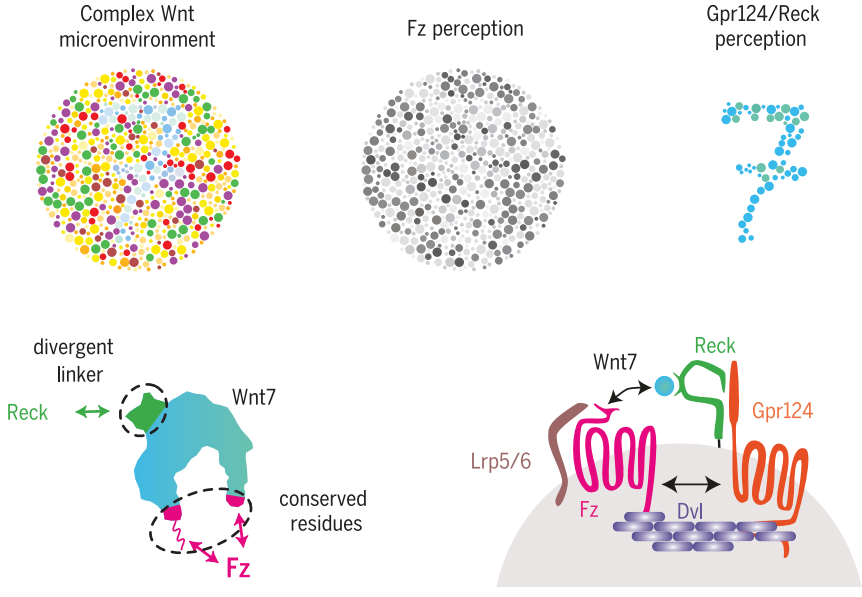

Task sharing for orchestrated Wnt7-specific cellular responses. (Top) Gpr124 and Reck cooperatively alter the cell's perception of its Wnt microenvironment by selectively potentiating Wnt7 signals (cyan-tinted dots). (Bottom) Reck decodes Wnt ligands by establishing monospecific contacts with the highly divergent Wnt7 linker domain. Gpr124 links Reck-bound Wnt7 to Dishevelled. Dishevelled polymers by interacting simultaneously with Gpr124 and Fz assemble Wnt7-enriched signalosomes that trigger signaling through Fz receptors and Lrp5/6 co-receptors.

The list of author affiliations is available in the full article online.
*These authors contributed equally to this work.
†Corresponding author. Email: benoit.vanhollebeke@ulb.ac.be
Cite this article as M. Eubelen *et al.*, *Science* **361**, eaat1178 (2018). DOI: 10.1126/science.aat1178

RESEARCH ARTICLE

DEVELOPMENTAL SIGNALING

A molecular mechanism for Wnt ligand-specific signaling

Marie Eubelen[1]*, Naguissa Bostaille[1]*, Pauline Cabochette[1], Anne Gauquier[1], Patricia Tebabi[1], Andra C. Dumitru[2], Melanie Koehler[2], Philipp Gut[1]†, David Alsteens[2], Didier Y. R. Stainier[3], Abel Garcia-Pino[4,5], Benoit Vanhollebeke[1,5,6]‡

Wnt signaling is key to many developmental, physiological, and disease processes in which cells seem able to discriminate between multiple Wnt ligands. This selective Wnt recognition or "decoding" capacity has remained enigmatic because Wnt/Frizzled interactions are largely incompatible with monospecific recognition. Gpr124 and Reck enable brain endothelial cells to selectively respond to Wnt7. We show that Reck binds with low micromolar affinity to the intrinsically disordered linker region of Wnt7. Availability of Reck-bound Wnt7 for Frizzled signaling relies on the interaction between Gpr124 and Dishevelled. Through polymerization, Dishevelled recruits Gpr124 and the associated Reck-bound Wnt7 into dynamic Wnt/Frizzled/Lrp5/6 signalosomes, resulting in increased local concentrations of Wnt7 available for Frizzled signaling. This work provides mechanistic insights into the Wnt decoding capacities of vertebrate cells and unravels structural determinants of the functional diversification of Wnt family members.

Wnts constitute a large family of highly conserved and secreted proteins that mediate intercellular communication during animal development and in adult tissue homeostasis (*1*, *2*). The 10 members of the Frizzled (Fz) family are seven-pass transmembrane proteins that serve as receptors for Wnts (*3*–*5*). Greatly contributing to the complexity of Wnt signaling, the Wnt/Fz binding relationships are promiscuous, with multiple Wnts competing for binding to individual Fzs and vice versa (*3*–*12*). The Wnt/Fz contacts are mediated by conserved residues or common chemical modifications (*13*). These observations raise the question of how cells can respond to specific Wnt ligands when exposed to the overlapping expression patterns of multiple Wnt ligands that sometimes have opposing biological functions.

A pertinent example is the exclusive control of mammalian forebrain and ventral spinal cord angiogenesis by Wnt7a and Wnt7b (*14*–*16*). Specifically, in order to respond to neural progenitor–derived Wnt7 by activating Wnt/β-catenin signaling, endothelial cells must express Gpr124, an orphan member of the adhesion class of G protein–coupled receptors (GPCRs) (*17*–*22*) as well as the glycosylphosphatidylinositol (GPI)–anchored glycoprotein Reck (*22*, *24*). Gpr124 and Reck physically interact to synergistically stimulate Wnt7-specific responses (*22*, *24*), but it is unknown how Wnt7 signals are specifically recognized and transduced.

Reck is a Frizzled-independent Wnt7-specific receptor

We first sought to determine the Wnt7 recognition mechanism, a question inherently complicated by the ubiquitous expression of Fz receptors and their Lrp5/6 co-receptors in vertebrate cells. We therefore generated a set of mutant human embryonic kidney (HEK)–293 cell lines by targeting (i) all 10 *FZ* genes ($FZ_{1\text{-}10}^{-/-}$), (ii) *LRP5* and/or *LRP6*, or (iii) *GPR124* and *RECK*, through multiplexed CRISPR/Cas9 mutagenesis (Materials and methods, Fig. 1A, and figs. S1 to S3). Ectopically expressed V5-tagged Wnt7a (Wnt7a-V5) could be immunodetected at the plasma membrane of wild-type (WT), $FZ_{1\text{-}10}^{-/-}$, and $LRP5^{-/-};LRP6^{-/-}$ cells but not $GPR124^{-/-};RECK^{-/-}$ cells (Fig. 1B). Ectopic restoration of Reck, alone or in combination with Gpr124, was sufficient to restore Wnt7a-V5 membrane labeling of $GPR124^{-/-};RECK^{-/-}$ cells (Fig. 1C). Fz5 also bound Wnt7a-V5, reflecting the competence of this receptor to mediate baseline Wnt7 signaling (*11*, *24*). Control Wnt3a-V5 did not label WT or mutant cells (Fig. 1B and fig. S4).

Proximity ligation assays (PLAs) allow localized detection of protein interactions at the single-molecule level through DNA rolling-circle signal amplification. PLAs in $GPR124^{-/-};RECK^{-/-}$ cells confirmed the interaction between Wnt7a-V5 and hemagglutinin (HA)–Reck or HA-Fz5 at the plasma membrane. The fraction of PLA-positive cells was identical (28.8 ± 7.5% and 28.3 ± 7.0%, respectively), but the intensity of the PLA signals generated with HA-Reck was twofold higher than with HA-Fz5 (Fig. 1D) (quantification protocol is provided in Materials and methods). By contrast, HA-Gpr124 did not generate PLA signals. We tested all the Wnt family members and found that PLA interaction signals with HA-Reck were restricted to Wnt7a-V5 and Wnt7b-V5 (Fig. 1E), reflecting the specificity of the Gpr124/Reck complex for Wnt7 signaling (*20*–*22*, *24*).

We next determined whether Reck recruits Wnt7a in the absence of functional Fz receptors. We first performed PLAs between V5-tagged Wnt7a or Wnt3a secreted from WT cells and HA-Reck exposed at the surface of neighboring green fluorescent protein (GFP)–labeled $FZ_{1\text{-}10}^{-/-}$ cells. PLA signals were detected at the plasma membrane of 57.7 ± 17.4% of the GFP^+ cells in $Wnt7a^+$ cocultures but were undetectable in $Wnt3a^+$ cocultures (Fig. 1F). Accordingly, the coculture of $FZ_{1\text{-}10}^{-/-}$ cells expressing Reck but not $Gpr124^{\Delta ICD}$ could drastically reduce Wnt7a-Fz5 signaling in neighboring Super Top Flash (STF) reporter cells (Fig. 1G). By contrast, none of the other tested Wnts, including Wnt3a (Fig. 1G), could be trapped by Reck-expressing cells (fig. S5). In this ligand capture assay, Gpr124 was lacking most of its C-terminal intracellular domain (ICD) domain (residues 81 to 337 of the ICD) to restrict the analysis to the extracellular parts of the Gpr124/Reck complex.

Defining the Reck-Wnt7 monospecific recognition mechanism

Next, we mapped the domains of Reck required for Wnt7a binding. We generated a collection of HA-tagged single-domain deletion variants of Reck and, after determining that all variants reached the plasma membrane (fig. S6), quantified Wnt7 PLA interaction signals. This analysis revealed that the N-terminal cysteine-knot domain (CK), and more particularly CK4 and CK5, were required for binding (Fig. 2A). Consistent with these results, $Reck^{\Delta CK4}$ was also inactive in competition assays (Fig. 1G).

Reck function in Wnt signaling is known to rely on its capacity to form a complex with Gpr124 through its CK domain (*22*, *24*), which we show to be required for Wnt7a binding. Although Gpr124 alone did not bind Wnt7 (Fig. 1, C, D, and G), we detected a fourfold increase in Wnt7a-V5/HA-Reck PLA signals upon coexpression of untagged Gpr124 (Fig. 2B). These results suggest that Reck is a Fz-independent Wnt receptor, whose specific and exclusive binding to Wnt7 is reinforced by the interaction of Gpr124 with its CK domain (Fig. 2C) (*24*).

In order to better characterize the Reck/Wnt7 interaction, we modeled the three-dimensional (3D) structure of Wnt7a based on *Xenopus* Wnt8a crystallographic analysis (Fig. 2D) (*13*). Wnt

[1]Laboratory of Neurovascular Signaling, Department of Molecular Biology, ULB Neuroscience Institute, Université libre de Bruxelles (ULB), Gosselies B-6041, Belgium. [2]NanoBiophysics Laboratory, Louvain Institute of Biomolecular Science and Technology, Université catholique de Louvain, 1348 Louvain-la-Neuve, Belgium. [3]Department of Developmental Genetics, Max Planck Institute for Heart and Lung Research, 61231 Bad Nauheim, Germany. [4]Laboratory of Cellular and Molecular Microbiology, Department of Molecular Biology, ULB, Gosselies B-6041, Belgium. [5]Walloon Excellence in Life Sciences and Biotechnology (WELBIO), Belgium. [6]Center for Microscopy and Molecular Imaging (CMMI), ULB, Gosselies B-6041, Belgium.
*These authors contributed equally to this work. †Present address: Nestlé Institute of Health Sciences, EPFL Innovation Park, Lausanne, Switzerland.
‡Corresponding author. Email: benoit.vanhollebeke@ulb.ac.be

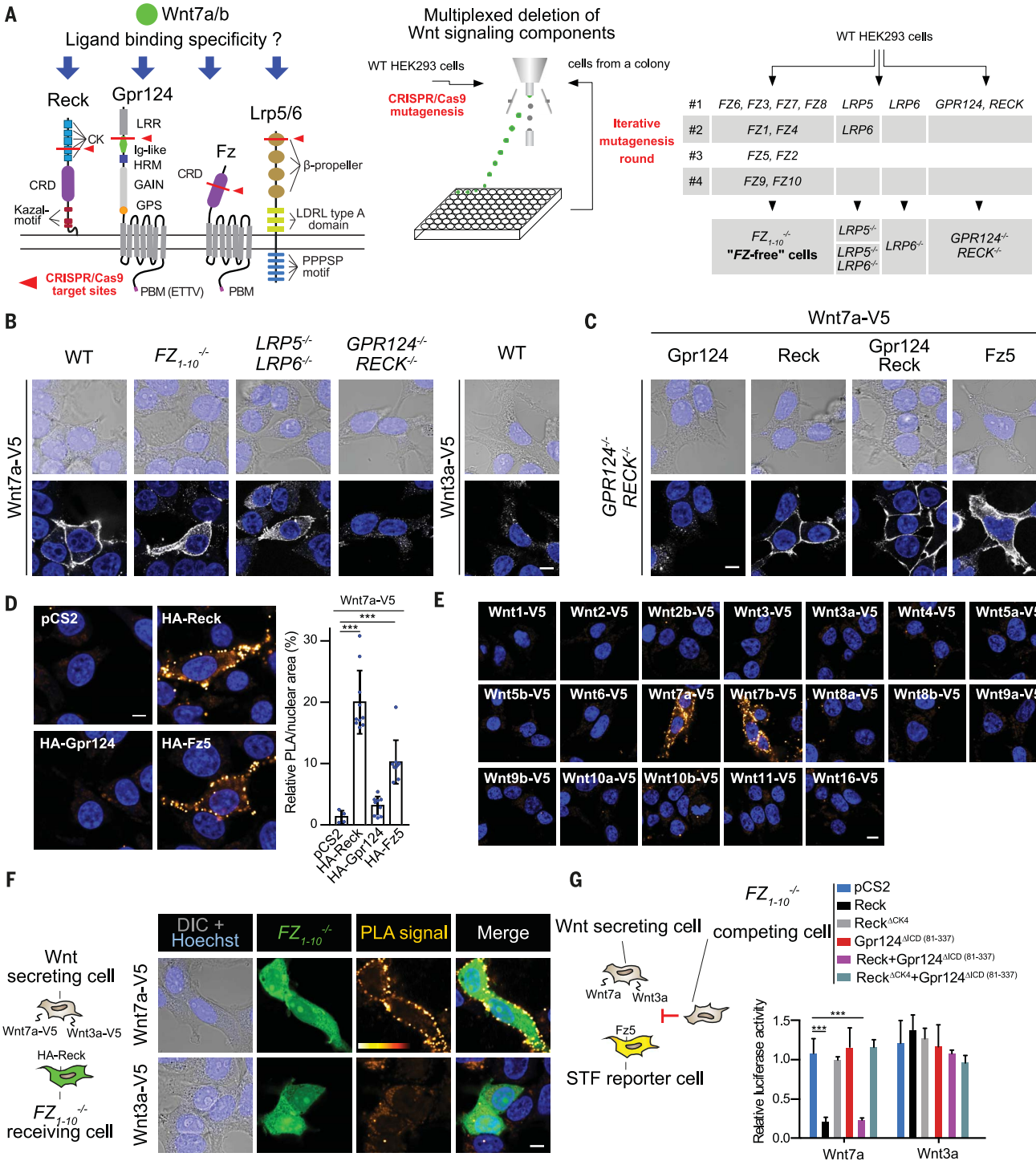

Fig. 1. Reck is a Frizzled-independent Wnt7-specific receptor. (**A**) Schematics of the Wnt7 receptor complex components and strategy for their genetic inactivation. Cells transfected with a bicistronic construct encoding the sgRNA and SpCas9-2A-GFP were iteratively cloned by means of fluorescence-activated cell sorting (FACS) (*49*). (**B**) Anti-V5 immunostaining of transiently expressed Wnt7a-V5 or Wnt3a-V5 in cells of the indicated genotype. (**C**) Same as (B) for cells transiently coexpressing Wnt7a-V5 and the indicated receptors and co-receptors. (**D**) PLA using antibody to V5 and antibody to HA directed against Wnt7a-V5 and the indicated HA-tagged receptors and co-receptors expressed in *GPR124*$^{-/-}$;*RECK*$^{-/-}$ cells. Signal quantification is on the right (Materials and methods). (**E**) Anti-V5/HA PLAs between the indicated V5-tagged Wnt ligand and HA-Reck in *GPR124*$^{-/-}$;*RECK*$^{-/-}$ cells. (**F**) Anti-V5/HA PLAs in (1:1) cocultures of Wnt7a-V5– or Wnt3a-V5–secreting WT cells and *FZ*$_{1\text{-}10}$$^{-/-}$ HEK293T cells coexpressing HA-Reck and cytosolic GFP as a transfection marker. (**G**) Ligand capture assay in triple (1:1:1) cocultures. Luciferase activities of HEK293-STF reporter cells transfected with Fz5 (yellow cell) and stimulated in a paracrine manner by cocultured Wnt7a- or Wnt3a-secreting cells in the presence of *FZ*$_{1\text{-}10}$$^{-/-}$ HEK293T competing cells transfected with various receptors and co-receptors as indicated. Scale bars, 10 μm. ***P < 0.001; data represent mean ± SD.

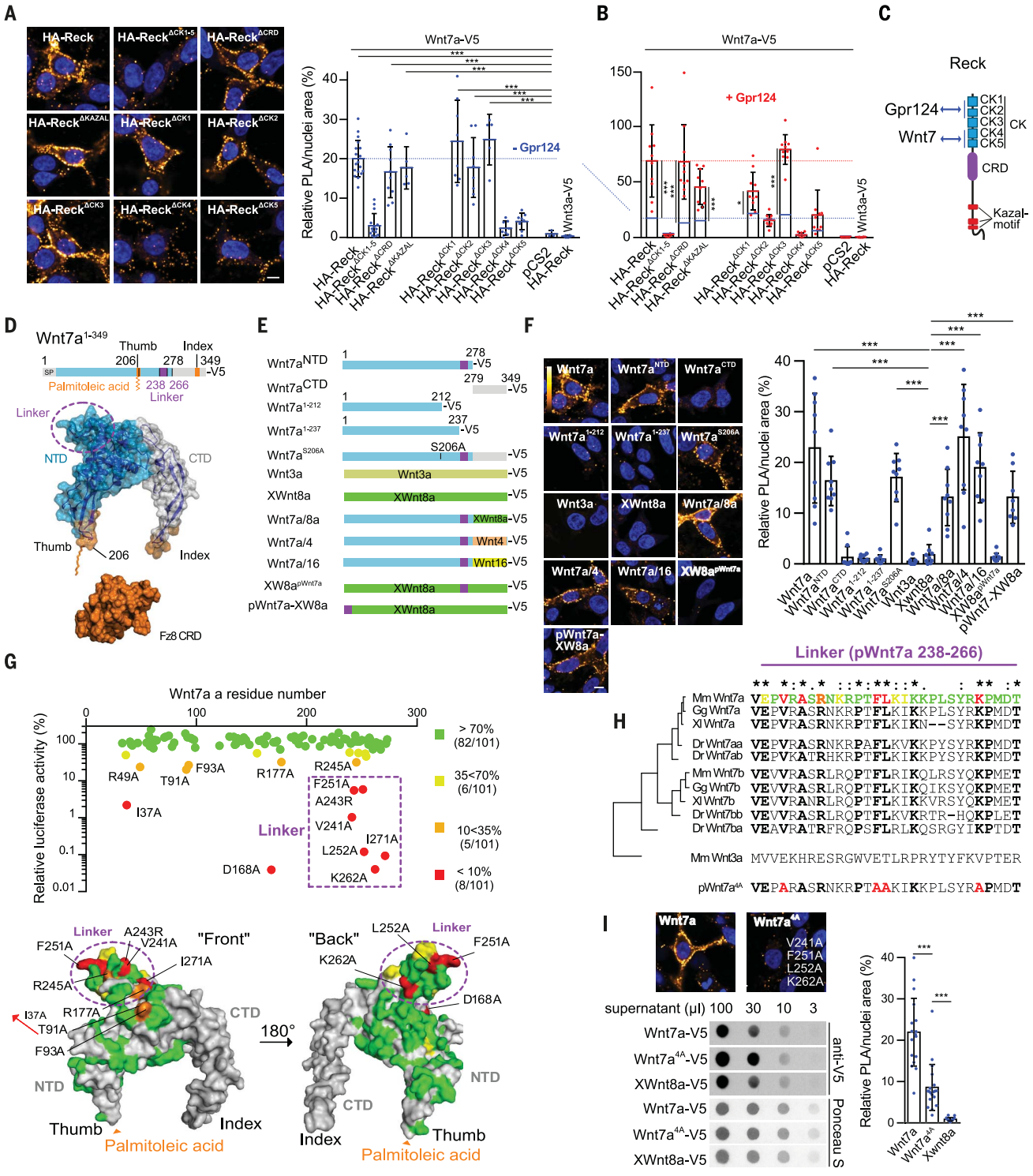

Fig. 2. Wnt7 recognition involves its intrinsically disordered linker region. (**A**) Anti-V5/HA PLAs between Wnt7a-V5 and HA-Reck or its variants coexpressed in *GPR124*$^{-/-}$;*RECK*$^{-/-}$ cells in the absence of Gpr124. Quantification is shown on the right. (**B**) Quantification as in (A) in the presence of Gpr124. (**C**) Reck and its Gpr124 and Wnt7 binding partners. (**D**) Structural modeling of Wnt7a based on the crystal coordinates of XWnt8a. The NTD and CTD are pseudocolored in cyan and gray, respectively. The NTD-embedded linker region is circled in purple. (**E**) Schematic representation of the V5-tagged Wnt variants examined in the anti-V5/HA PLAs shown and quantified in (**F**) in *GPR124*$^{-/-}$;*RECK*$^{-/-}$ cells coexpressing HA-Reck. (**G**) Gpr124/Reck–dependent luciferase activities of 101 different single-residue variants of Wnt7a normalized to WT Wnt7a in HEK293-STF cells. (**H**) Alignment of the Wnt7 linker domain across the vertebrate clade. Mm, *Mus musculus*; Gg, *Gallus gallus*; Xl, *Xenopus laevis*; Dr, *Danio rerio*. The residues of Mm Wnt7a are color-coded according to their activity class determined in (G). (**I**) Anti-V5/HA PLAs between Wnt7a-V5 or Wnt7a^{4A}-V5 and HA-Reck. Ligand secretion was evaluated by means of semiquantitative anti-V5 dot blot analysis of serially diluted cell supernatant. Ponceau S staining was used as the loading control. Scale bars, 10 µm. *P < 0.05, ***P < 0.001; data represent mean ± SD.

ligands adopt a two-domain structure reminiscent of a human hand pinching the globular Fz cysteine-rich domain (CRD) (Fig. 2D, orange) via the palmitoylated "thumb" of their N-terminal domain (NTD) (Fig. 2D, cyan) and hydrophobic residues of their "index" C-terminal domain (CTD) (Fig. 2D, gray). The structures involved in Fz binding are pseudocolored in orange in Fig. 2D. The two domains are connected through a flexible linker region of the NTD (Fig. 2D, purple).

We next generated a collection of Wnt7 variants deleted for specific domains or residues or that carried domains from other Wnt ligands (Fig. 2E). All analyzed Wnt7 variants could be detected in the cell supernatant (fig. S7). These ligands were each applied to PLAs, and the resulting data showed that Reck binding occurs through the Wnt7a NTD. Wnt7a^{NTD} indeed bound Reck, whereas Wnt7a^{CTD} did not (Fig. 2F). Chimeric ligands made of Wnt7a^{NTD} fused to the CTDs of *Xenopus* Wnt8a (XWnt8a) or mouse Wnt4 or Wnt16 were also positive. The palmitoleic acid required for Fz binding was dispensable for the interaction with Reck, as revealed through testing a Wnt7a^{S206A} palmitoylation mutant. Altogether, these binding assays reveal that Reck discriminates between Wnt ligands by recognizing a motif embedded in the Wnt7a NTD at sites distinct from those engaged by Fz.

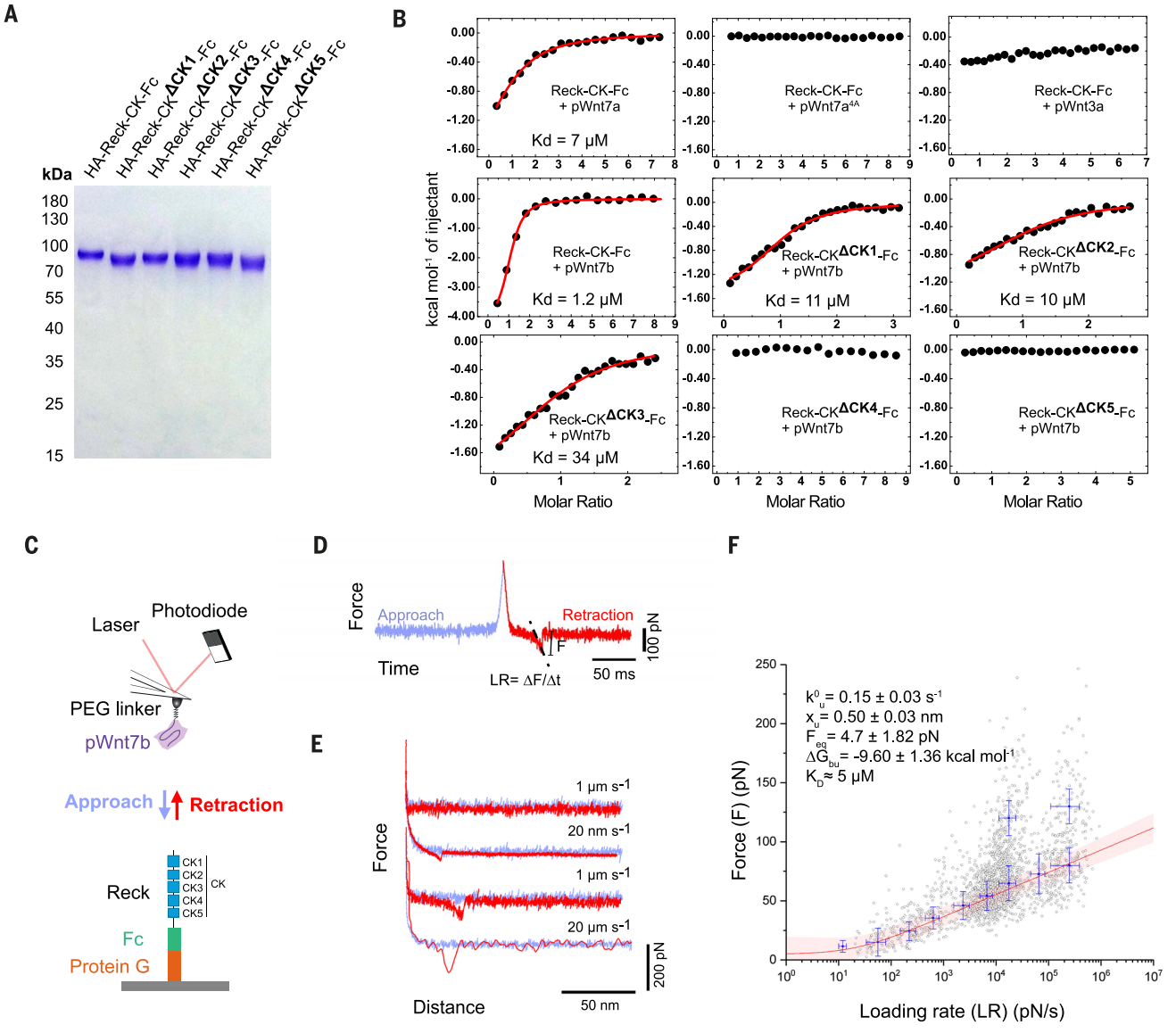

Fig. 3. The Wnt7 linker peptide binds the Reck CK domain with low micromolar affinity. (**A**) Coomassie Blue staining of the recombinant Reck-CK-Fc fusion proteins used in biophysical analyses. (**B**) Interaction between Reck-CK-Fc and synthetic pWnt7 peptides by use of isothermal titration calorimetry (ITC). (Top) ITC of pWnt7a, pWnt7a^{4A}, and pWnt3a into Reck-CK-Fc. (Middle and bottom) ITC of Reck-CK-Fc and its CK motif variants to pWnt7b. (**C**) Probing Reck-CK-Fc/pWnt7b interaction by use of SMFS. Principle of force-distance curve-based atomic force microscopy (FD-based AFM) is shown. An AFM tip functionalized with a polyethylene glycol (PEG) spacer fused to the pWnt7b peptide is approached and retracted from a surface coated with Reck-CK-Fc. (**D**) Force-time curve from which the loading rate (LR) can be extracted from the slope of the curve just before bond rupture (LR = $\Delta F/\Delta t$). (**E**) Force-distance curves recorded at various retraction speeds (from 20 nm s^{-1} to 20 μm s^{-1}) and showing no adhesion event (first curve) or specific adhesion events (other curves). (**F**) Loading rate–dependent interaction forces of single Wnt7b peptide-receptor bonds quantitate the ligand-binding energy landscape of Reck. (Inset) Fitting the data by using the Friddle-Noy-de Yoreo model (thin red line) (*54*) provides average equilibrium force (F_{eq}), barrier location of the unbound state (x_u), equilibrium free energy between the bound and unbound state (ΔG_{bu}), intrinsic unbinding rate (k^0_u), and K_d, with errors representing the S.E.. Each circle represents one measurement. Darker shaded areas represent 95% prediction interval.

Smaller NTD variants lacking the linker region, $Wnt7a^{1-212}$ and $Wnt7^{1-237}$, did not bind Reck. This mutational analysis and the spatial segregation of the Wnt7a linker region from the Fz binding sites suggest that Reck decodes Wnt7a, at least in part, through this linker. The linker, which is highly divergent among the different Wnt ligands, exhibits strong evolutionary conservation among the vertebrate Wnt7 orthologs (Fig. 2H and fig. S8). This region is predicted to be intrinsically disordered (fig. S9), a feature often found in molecular recognition elements providing the necessary structural plasticity to accommodate multiple partners, post-translational modifications, or moonlighting functions. In many cases, intrinsically disordered regions also provide interactions with high specificity and moderate-to-high affinity (*25*).

Although in situ substitution of the XWnt8a linker by the Wnt7 linker ($XW8a^{pWnt7a}$) did not yield detectable PLA signals, presenting the Wnt7 linker at the free N terminus of XWnt8a (pWnt7a-XW8a) was sufficient to confer Reck binding activity to XWnt8a (Fig. 2, E and F). We hypothesize that conformational alteration accounts for the lack of binding of $XW8a^{pWnt7a}$. In support of this hypothesis, reciprocal exchange of Wnt linkers between various Wnts abrogates their activity (fig. S10).

To precisely map the Reck interaction site, we analyzed Gpr124/Reck–dependent STF signaling of 101 single-residue variants of Wnt7a (Fig. 2G). The mutated residues correspond to surface-exposed NTD residues conserved between Wnt7a and Wnt7b but not found in XWnt8a or other Wnt ligands. Residues were mutated to alanines, except for endogenous alanine residues, which were changed to arginine. Although ~80% of the variants were as active as WT Wnt7a (>70% relative activity) (Fig. 2G, green), eight Wnt7a variants (Fig. 2G, red) reduced Gpr124/Reck–dependent signaling to <10%. All but one (I37) critical residues clustered on the "top" or "back" of the predicted Wnt7a structure, with six mapping to the linker domain. All essential residues are strictly conserved among Wnt7 orthologs from fish to mammals and absent in other Wnts, including Wnt3a (Fig. 2H and fig. S8).

The linker domain of Wnt3a has been shown to be essential for Wnt3a activity through Lrp6 binding (*26*). By analogy, the inactivity of the Wnt7 linker variants might therefore result from defective binding to Lrp5/6, Reck, or both. In line with a function in Reck binding, $Wnt7a^{4A}$, a four-residue variant of Wnt7a (V241A/F251A/L252A/K262A) within the linker region (Fig. 2H), showed reduced Reck PLA signals as compared with that of WT Wnt7a. This lower activity occurred despite slightly improved secretion rates (Fig. 2I).

Biophysical characterization of the interaction between the Wnt7 linker domain and Reck

To investigate Reck-Wnt7 binding in a cell-free system, the CK domain of Reck (and variants thereof) were fused to the Fc domain of human immunoglobulin G1 (IgG1). Fusion proteins were purified from HEK293T cells supernatants (Fig. 3A) and then titrated with synthetic pWnt7a and pWnt7b linker peptides by means of isothermal titration calorimetry (ITC). pWnt7a and pWnt7b bound Reck with affinity values of 7 and 1.2 μM, respectively (Fig. 3B and fig. S11). As controls, the synthetic peptides corresponding to $Wnt7a^{4A}$ ($pWnt7a^{4A}$) as well as equivalent linker peptides of Wnt3a (pWnt3a) showed no binding to Reck-CK-Fc. pWnt7b binding required Reck CK4 and CK5 but not CK1, CK2, or CK3, mirroring the PLA results in cultured cells (Fig. 2A). To corroborate the results provided by the ITC analysis, we used single-molecule force spectroscopy (SMFS) to measure binding affinities at the single-molecule level (Fig. 3C). Binding of pWnt7b to Reck-CK-Fc was detectable with a measured dissociation constant (K_d) of 5 μM (Fig. 3, D to F). Despite the fundamental differences between the two techniques, ITC and SMFS thus provided a close match between measured binding affinity values.

Altogether, although not excluding an additional role of the Wnt7 linker in Lrp5/6 binding (*26*), these data demonstrate that Wnt7 is recognized by Reck at least in part through its "signature" linker motif. The moderate micromolar affinity values measured further suggest that after recognition of the linker, Reck establishes more extensive contacts with Wnt7, in a process that can be potentiated by Gpr124 (Fig. 2B).

Gpr124 function in Wnt7 signaling does not depend on its GPCR structure

Reck, by virtue of its GPI-anchoring mode, has limited potential to relay Wnt7 signals within the cell. Signal transduction therefore likely relies on other components of the receptor complex—Gpr124 and/or Fz/Lrp5/6 (Fig. 4A).

To uncover the signal transduction mechanism, we first evaluated the functional relationship between Gpr124 and Fz/Lrp5/6 complexes in cultured cells. Using the Fz and Lrp mutant cells (Fig. 1A), we found that the function of Gpr124/Reck strictly relies on Fz and Lrp5/6 (fig. S12). We further established that their respective CRD and Dkk-1–sensitive Wnt ligand-binding domains are essential, implying that Wnt7 binds and activates Fz/Lrp5/6 in a classical manner. If Reck mediates Wnt7 binding and Fz/Lrp5/6 trigger signaling, what underlies the essential function of Gpr124?

In the absence of Gpr124, Reck acts cell-autonomously as a potent inhibitor of Wnt7/Fz5 signaling, in a CK4-dependent manner (Fig. 4B). The inhibitory function of standalone Reck is particularly remarkable in light of the pool of membrane-associated Wnt7 in this Frizzled-positive setting (Fig. 4B). This observation implies that in the absence of Gpr124, Reck scavenges Wnt7 away from Fz5/Lrp5/6 complexes. The presence of Gpr124 switches Wnt7 signaling output from near complete inhibition to potent activation.

To establish how Gpr124 mediates this "on-off" Wnt7 signaling switch, we turned to the zebrafish model. In many Wnt-controlled processes, including the Wnt7/Gpr124/Reck–mediated cerebrovascular functions, Wnt input levels are only marginally above the minimal threshold values required for signaling (*20*). It is therefore important to investigate the signal transduction pathway in vivo, in response to physiological Wnt7 inputs. The development of the zebrafish brain vasculature requires Reck/Gpr124 signaling in a process of angiogenic sprouting that can readily be quantified. It therefore constitutes an ideal setting in which to perform structure-function analysis in vivo (*22*, *27*). Using mRNA injections into one-cell stage *gpr124*$^{-/-}$ embryos (Fig. 4C), we evaluated the activity of three Gpr124 variants lacking the N-terminal extracellular part ($Gpr124^{\Delta ECD}$), the seven-span moiety ($Gpr124^{\Delta TM2\text{-}7}$), or the C-terminal cytoplasmic extension ($Gpr124^{\Delta ICD}$, lacking residues 29 to 337 of the ICD) (Fig. 4D). Although ectopic expression of $Gpr124^{\Delta ECD}$ or $Gpr124^{\Delta ICD}$ did not restore brain angiogenesis in *gpr124* mutants or morphants, $Gpr124^{\Delta TM2\text{-}7}$ was sufficient to trigger brain angiogenesis in vivo (Fig. 4, E and F, and fig. S13) and Wnt/β-catenin activity in vitro (fig. S14).

This retained competence of $Gpr124^{\Delta TM2\text{-}7}$ was unexpected: Gpr124 is a GPCR, a receptor superfamily classically relaying extracellular stimuli through ligand-induced conformational remodeling of their seven transmembrane spans, which are absent in the engineered $Gpr124^{\Delta TM2\text{-}7}$. These data raise the possibility that Gpr124 does not act as a "classical" GPCR when promoting Wnt7 signaling.

To test this hypothesis, we developed a bimolecular complementation assay in which the GPR124 extracellular domain (ECD) and ICD are linked by a surrogate anti-GFP VhhGFP4 nanobody-GFP connector (Fig. 4G). Nanobodies are single-domain antibody fragments that have been used to rout or misrout intracellular proteins (*28*). We repurposed them here as conditional tethers for signal transduction analysis. The highly flexible GFP-VhhGFP4 connector acts a buffering module, ensuring that conformational information cannot be exchanged between tethered partners. On the basis of this idea, we designed $Gpr124^{\Delta ICD}$-GFP and $Gpr125^{\Delta ICD}$-GFP fusions to which VhhGFP4 fusions will be recruited (Fig. 4G and fig. S15). The *gpr124* vascular phenotypes were partially suppressed by co-injecting mRNAs encoding $Gpr124^{\Delta ICD}$-GFP and VhhGFP4-ICD (residues 29 to 337) (Fig. 4H). Moreover, a chimeric Gpr124 ECD linked to cytoplasmic GFP via the transmembrane span of the unrelated CD27 receptor was similarly active with VhhGFP4-ICD (Fig. 4, G and H). We used Gpr125, a closely related aGPCR devoid of angiogenic activity, as well as VhhGFP4–red fluorescent protein (RFP) as negative controls (*20*–*22*).

These results confirm that Gpr124 function in Wnt7 signaling does not require signal transduction across the membrane through conformational remodeling. Instead, Gpr124 seemingly acts in this module as a signaling-deficient transmembrane protein whose activity relies on its Reck-binding ECD (*22*, *24*) and its conformationally

uncoupled ICD. The function of this latter domain remains to be defined (Fig. 4I).

Gpr124 activity requires Dishevelled binding

We hypothesized that the Gpr124 ICD might operate through Dishevelled (Dvl), the necessary effector of Wnt signaling that interacts with Fz. This "Dvl hypothesis" is rooted in the findings that Gpr125 physically interacts with Dvl via its C-terminal ICD domain (*29*) and that Gpr124/125 hybrids in which the ICD of Gpr124 is replaced with the ICD of Gpr125 are able to promote brain angiogenesis (Fig. 5A) (*22*). Gpr124/Fz2 hybrids ($Gpr124^{ICDFz2}$) harboring the Fz2 ICD, which is known to bind Dvl, were similarly active. By contrast, full-length Fz2 was not. The activity of $Gpr124^{ICDFz2}$ was dependent on its KTxxxW and ETTV Dvl binding motifs (Fig. 5A).

Moreover, in a noncanonical Wnt signaling context, overexpression of Gpr125 impairs

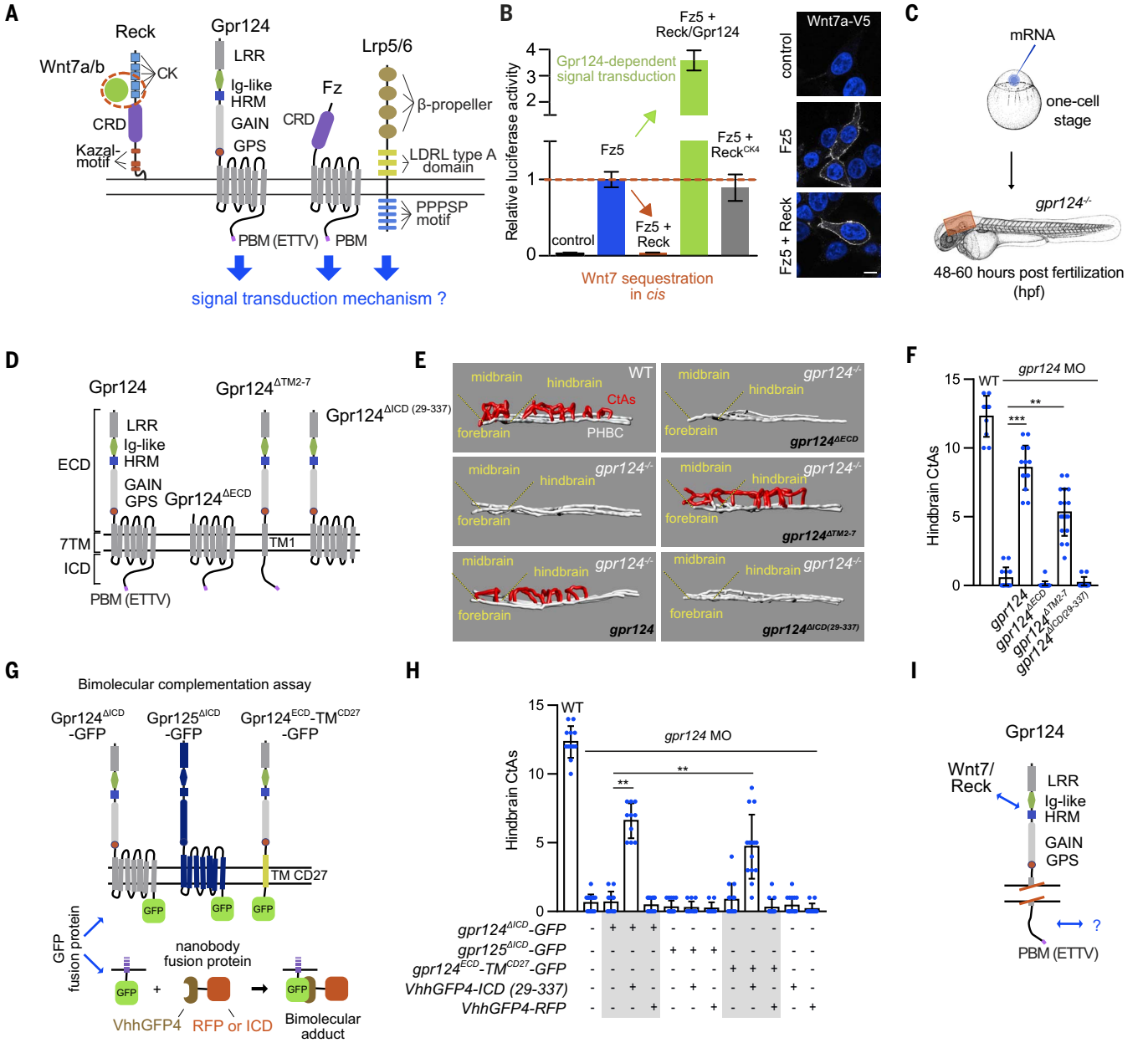

Fig. 4. Gpr124 function in Wnt signaling does not depend on its GPCR structure. (**A**) Potential Wnt7-specific signal transduction mechanisms. (**B**) Luciferase activity (left) and anti-V5 immunostaining (right) of HEK293-STF cells cotransfected with Fz5, Wnt7a, and the indicated receptors and co-receptors. (**C**) Experimental setup for in vivo brain angiogenesis assays in zebrafish embryos after RNA injections at the one-cell stage. The red area is imaged to analyze the hindbrain central arteries (CtAs). (**D**) Gpr124 and its domain variants. (**E**) Representative 3D wire diagrams of the cerebrovasculature of WT and *gpr124* mutant embryos at 60 hours post fertilization, injected with 100 pg of the indicated RNA. Red vessels represent the Gpr124/Reck–dependent intracerebral CtAs that sprout from the gray perineural primordial hindbrain channels (PHBCs); the confocal stacks used to generate the wire diagrams are available in fig. S13. (**F**) Hindbrain CtAs of *gpr124* morphant embryos at 60 hours post fertilization, injected at the one-cell stage with 100 pg of the indicated mRNA. (**G**) Bimolecular GPCR complementation assay strategy. Membrane receptors (Gpr124, Gpr125, and $Gpr124^{ECD}$-TM^{CD27}) inactivated by ICD/GFP substitutions are coexpressed with VhhGFP4 fusions to reconstitute a bimolecular adduct through an artificial GFP-VhhGFP4 linker. (**H**) Hindbrain CtAs of *gpr124* morphant embryos at 60 hours post fertilization, injected at the one-cell stage with 100 pg of the indicated mRNAs. (**I**) Gpr124 and its essential protein interactions. Scale bar, 10 μm. $^{**}P < 0.01$, $^{***}P < 0.001$; data represent mean ± SD.

convergence and extension movements during zebrafish gastrulation, resulting in a mediolateral broadening of the anterior-posterior embryonic axis as well as synophthalmia or cyclopia (*29*). These phenotypes were linked to the capacity of Gpr125 to modulate Dvl distribution through its ICD. Gpr124 strictly mimicked Gpr125 in these settings (Fig. 5B and fig. S16).

We therefore tested whether Gpr124 affects the intracellular distribution of Dvl. We used two distinct cell populations of the zebrafish blastula to address this question: the superficial enveloping layer (EVL) cells, which maintain continuous intercellular contacts, and the deep layer (DEL) cells, which establish more discrete

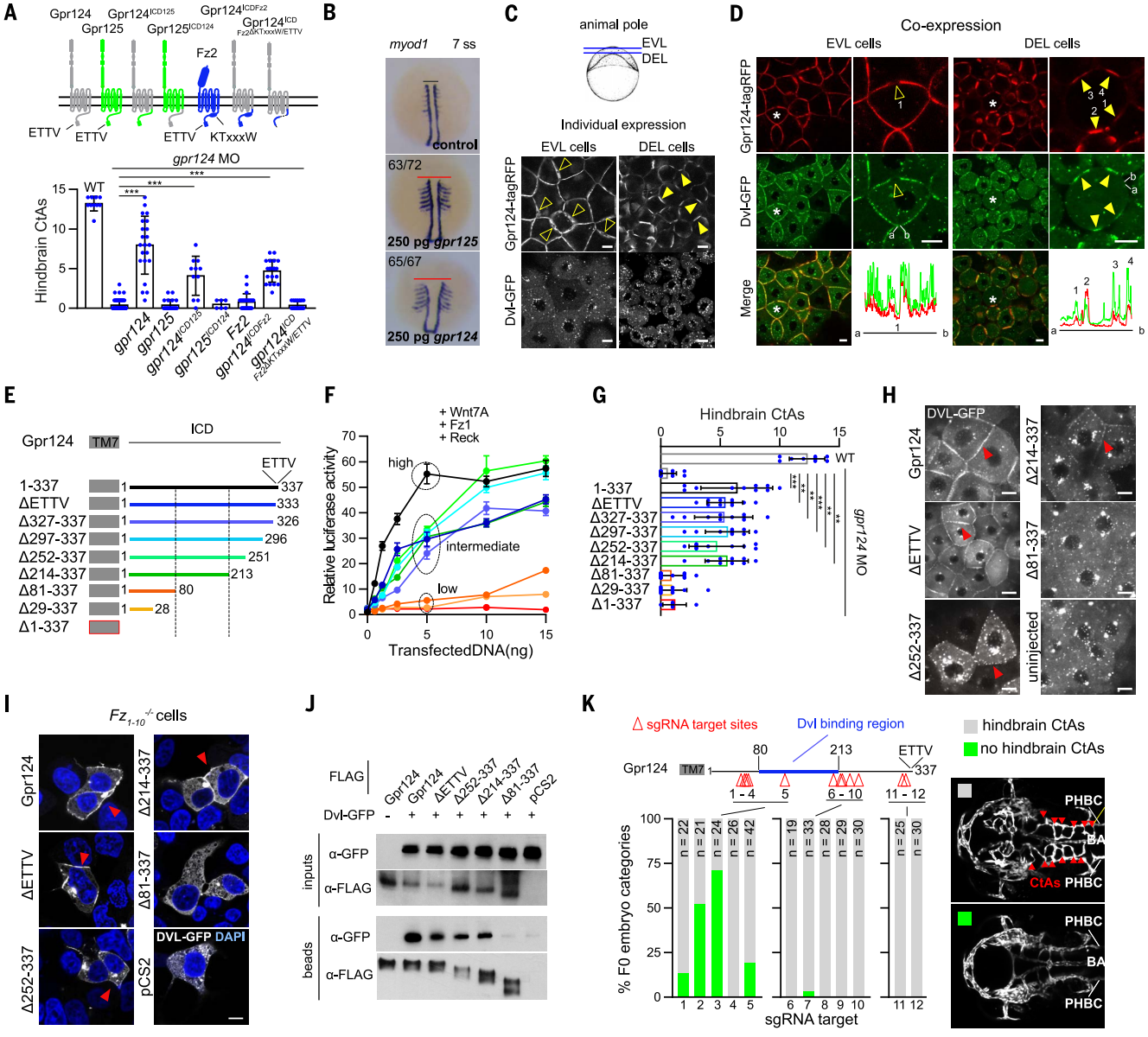

Fig. 5. Gpr124 interacts with Dvl through its ICD. (**A**) Hindbrain CtAs of *gpr124* morphant embryos at 60 hours post fertilization, injected at the one-cell stage with 100 pg mRNA encoding the illustrated receptors. (**B**) WISH of *myod1* expression at the seven-somite stage embryos, control, or injected with 250 pg of *gpr125* or *gpr124* mRNA. The red lines indicate the mediolateral broadening of the anterior-posterior axis. (**C**) Intracellular distribution of Gpr124-tagRFP and Dvl-GFP expressed individually in zebrafish blastulae. (**D**) Intracellular distribution of Gpr124-tagRFP and Dvl-GFP coexpressed in zebrafish blastulae. The cells annotated with an asterisk are magnified at right, and the pixel intensity of the green and red channels along a virtual clockwise path following the cell cortex from a to b is plotted below. In (C) and (D), open and solid arrowheads point respectively to Gpr124-negative and Gpr124-positive membrane microdomains in EVL and DEL cells. (**E**) Gpr124 and its ICD variants. (**F**) Luciferase dose-response values of HEK293-STF cells cotransfected with Wnt7a, Fz1, Reck, and increasing amounts of Gpr124 constructs or its ICD variants as illustrated in (E). (**G**) Hindbrain CtAs of *gpr124* morphant embryos at 60 hours post fertilization, injected at the one-cell stage with 100 pg of the indicated mRNA. (**H**) Intracellular distribution of Dvl-GFP coexpressed with Gpr124 and its ICD variants in zebrafish blastula EVL cells. (**I**) same as (H) in $FZ_{1\text{-}10}{}^{-/-}$ cells. In (H) and (I), red arrowheads point to Dvl-GFP signal at the plasma membrane. (**J**) Anti-FLAG coimmunoprecipitation assays in total lysates of cells coexpressing Dvl-GFP and N-terminal FLAG-tagged versions of Gpr124 or its ICD variants. (**K**) Mosaic gene disruption in somatic zebrafish embryos by means of injection at the one-cell stage of 150 pg of *zCas9* mRNA and 50 pg of the illustrated sgRNAs. Resulting hindbrain vasculature scored at 48 hours post fertilization. BA, Basilar artery. Scale bars, 10 μm. $^{**}P < 0.01$, $^{***}P < 0.001$; data represent mean ± SD.

intercellular junctions (Fig. 5C). Gpr124-tagRFP distribution reflects this differing junctional organization, with near-uniform membrane signals in EVL and discontinuous signals in DEL cells (Fig. 5C). When expressed individually, *Xenopus* Dvl-GFP mainly formed cytoplasmic punctae in both cell populations, as reported previously (*29*). Coexpressing Gpr124-tagRFP largely redistributed Dvl-GFP to the Gpr124-positive membrane subdomains in both EVL and DEL cells, where the proteins colocalized (Fig. 5D).

We generated a collection of Gpr124 truncation variants with a range of deletions within the 337-amino-acid-long ICD (Fig. 5E) and evaluated their Wnt7/β-catenin functions in vitro (Fig. 5F) and in vivo (Fig. 5G). The Gpr124 and Gpr125 ICDs contain no obvious motifs except for the last four ETTV amino acids that constitute a canonical PDZ-binding motif (PBM), which is also found in a subset of Fz receptors. The ETTV tetrapeptide contributed, but was not essential, for Gpr124 activity. It was similarly dispensable for high-dose Gpr124- or Gpr125-induced planar cell polarity phenotypes (fig. S16) (*29*). Analysis of increasingly larger C-terminal deletion variants mapped the essential region of the Gpr124 ICD to the interval spanning residues 80 to 213. The activity of the different ICD variants exactly matched their capacity to recruit Dvl-GFP in EVL cells (Fig. 5H) and $FZ_{1\text{-}10}^{-/-}$ cells (Fig. 5I). This interaction between Gpr124 and Dvl could also be detected with coimmunoprecipitation. In these assays, only Gpr124 variants harboring the 81–213 region interacted with exogenous Dvl-GFP (Fig. 5J) or endogenous DVL2 (fig. S17) in $FZ_{1\text{-}10}^{-/-}$ cells. This interaction is likely direct because purified recombinant GST-Gpr124-ICD or GST-Gpr124-$ICD^{\Delta ETTV}$ fusion proteins were able to pull down in vitro–translated Dvl-GFP (fig. S18), as previously reported for Gpr125 (*29*).

To test for the endogenous requirement for Gpr124 ICD interaction with Dvl, we performed gene-disruption experiments in somatic zebrafish embryos by coinjecting *zCas9* mRNA and single-guide RNAs (sgRNAs) targeting the Gpr124 coding sequence immediately upstream, within, or downstream of the Dvl-binding region (ICD residues 80 to 213). Although the injection of four out of five sgRNAs predicted to disrupt Dvl recruitment to Gpr124 generated embryos that lack hindbrain CtAs with a penetrance ranging from 13.6 to 70.8%, none of the seven sgRNAs targeting Gpr124 downstream of the Dvl-binding region generated penetrant brain vascular defects (Fig. 5K).

Taken together, these experiments identify Dvl as a Gpr124 binding partner that could mediate its Wnt7 signaling activities at the plasma membrane. Unlike Fz, Gpr124-mediated recruitment of Dvl at the plasma membrane did not yield a detectable increase in phosphorylated Dvl levels, an early indicator of Wnt signaling activation upstream of β-catenin stabilization (fig. S19) (*30*, *31*). This absence of Gpr124-induced Dvl activation is consistent with the experiments shown in Fig. 4, D to I, that demonstrated Gpr124 to be a conformationally inert Wnt7 signaling mediator.

Dvl polymers assemble ligand-specific Wnt signalosomes by linking Gpr124 and Fz

Knockdown of *DVL2* by means of small interfering RNA (siRNA) impairs Gpr124/Reck–mediated signaling (fig. S20). Because Dvl is an essential adaptor of Fz, and Gpr124/Reck signaling relies on Fz (fig. S12), such cell-wide loss-of-function approaches are however of limited value to probe Dvl function specifically as a Gpr124 (and not Fz) effector. We therefore used the nanobody strategy described in Fig. 4G to selectively modulate Dvl binding to Gpr124. VhhGFP4-mediated recruitment of Dvl to Gpr124$^{\Delta ICD}$-GFP, but not to Gpr125$^{\Delta ICD}$-GFP, was sufficient to partially reverse the *gpr124* mutant vascular phenotype in vivo (Fig. 6A). As additional control, injecting either component alone or substituting VhhGFP4-Dvl with VhhGFP4-RFP did not rescue brain angiogenesis. These experiments reveal that Dvl is sufficient to mediate Gpr124 intracellular functions in Wnt7 signaling.

Gpr124, Reck, and Fz/Lrp5/6 have been reported to form higher-order receptor complexes (*24*). We reasoned that the Gpr124 ICD might assemble this complex via Dvl. Dvl molecules indeed assemble signalosomes through dynamic polymerization (*32*–*34*). Because Dvl physically interacts with both Gpr124 and Fz, Gpr124 and the associated Reck-bound Wnt7 might thus become trapped in dynamic Wnt signalosomes, increasing the local concentration of Wnt7 ligands available for Fz signaling.

Wnt signalosomes are readily detected with light microscopy as large, punctate structures enriched in Dvl that form at or below the plasma membrane (*33*–*35*). To determine whether Fz and Gpr124 codistribute in Wnt signalosomes in a Dvl-dependent manner, we first examined the localization of individually expressed Fz-GFP and Gpr124-tagRFP in DEL cells. Fz4 decorated the entire plasma membrane periphery, whereas Gpr124-tagRFP accumulated at cellular contacts (Figs. 5, C and D, and 6B). This differential membrane localization was retained upon Dvl expression (Fig. 6B). Consistent with their Dvl binding capacity, both receptors recruited Dvl-GFP from the cytoplasm (Fig. 5C) to their respective membrane compartments (Fig. 6C). However, when Gpr124-tagRFP and Fz4-GFP were coexpressed, Fz4-GFP quantitatively relocalized, in a Dvl-dependent manner, to the Gpr124-positive intercellular junctions (Fig. 6D). Gpr124-tagRFP and Fz4-GFP colocalized in Wnt signalosome-reminiscent punctate structures that were particularly evident at EVL cell membranes (Fig. 6E and fig. S21).

We used bimolecular fluorescence complementation as an additional assay to test for Dvl-dependent Fz/Gpr124 interaction in DEL cells. Coinjection of Gpr124-VN_{155} (I152L) and Fz1-VC_{155} indeed generated bright junctional signals in a Dvl-dependent manner (Fig. 6F), demonstrating that Fz and Gpr124 indirectly interact via the Dvl scaffold protein. Altogether, these data provide a molecular mechanism for spatial enrichment of Wnt7 within Fz/Lrp5/6 signalosomes, permitting potentiated and ligand-selective cellular responses (Fig. 6G).

Discussion

This work provides mechanistic insights onto the Wnt decoding capacities of vertebrate cells. It also demonstrates that the evolutionarily constrained Wnt structure retained enough diversity to allow ligand-specific cellular responses, a property so far thought to require structurally unrelated Frizzled ligands such as Norrin (*36*).

These structural insights into Wnt evolution and function suggest that additional Wnt decoding modules exist, enabling fine-tuning of cellular behaviors in response to other Wnt or Fz family members. The discrete interaction mode of Fz and Wnt leaves large surfaces made of evolutionary conserved residues available to accommodate additional co-receptors. We therefore propose that Wnt decoding modules might have contributed to shaping the evolution of the Wnt ligand family.

The benefit to promiscuous Wnt/Fz interactions with specificity conferred by accessory proteins rather than monospecific Wnt/Fz interactions might lie in the increased modularity offered by the binary system. A single-component system would be limited to an on-or-off signaling output. The two-component system described here can, context-dependently, achieve cell-autonomous Wnt signaling inhibition or act as a tunable rheostat amplifying the signaling output of specific Wnt ligands.

A salient molecular property of the Wnt7 module is the use of Dvl as a common Gpr124 and Fz adaptor. It is tempting to propose that taking advantage of Fz-associated scaffold proteins such as Dvl could constitute a generic mechanism for Wnt/Fz modifiers. Accordingly, cells recurrently tailor their responses to Wnt by reshaping the molecular composition of the Dvl-associated proteins, including regulatory kinases, E3 ubiquitin ligases, and components of the endocytic machinery (*32*–*34*).

Our findings have clinical implications. The pleiotropic functions of Wnt signaling in health and disease make this pathway a conspicuous yet intrinsically challenging therapeutic target. Manipulating the Wnt/β-catenin pathway at the level of its cytosolic or nuclear components harbors high potential for systemic effects with undesirable outcomes across a range of tissues (*37*). Interventions focused on specific Wnts, Fz receptors, or other signaling components at the cell membrane might in principle be more selective and hence better positioned to lead to clinically viable strategies (*4*, *38*–*40*). The mechanism uncovered here expands the prospects for specific Wnt-targeted interventions. In particular, by giving molecular insights at the heart of Wnt7-specific signaling, it provides an opportunity for the targeted treatment of human brain disorders with neurovascular involvement, including stroke and brain cancer (*41*).

Materials and methods

Zebrafish lines

Zebrafish (*Danio rerio*) were maintained at 28°C on a 14 hours light/10 hours dark cycle.

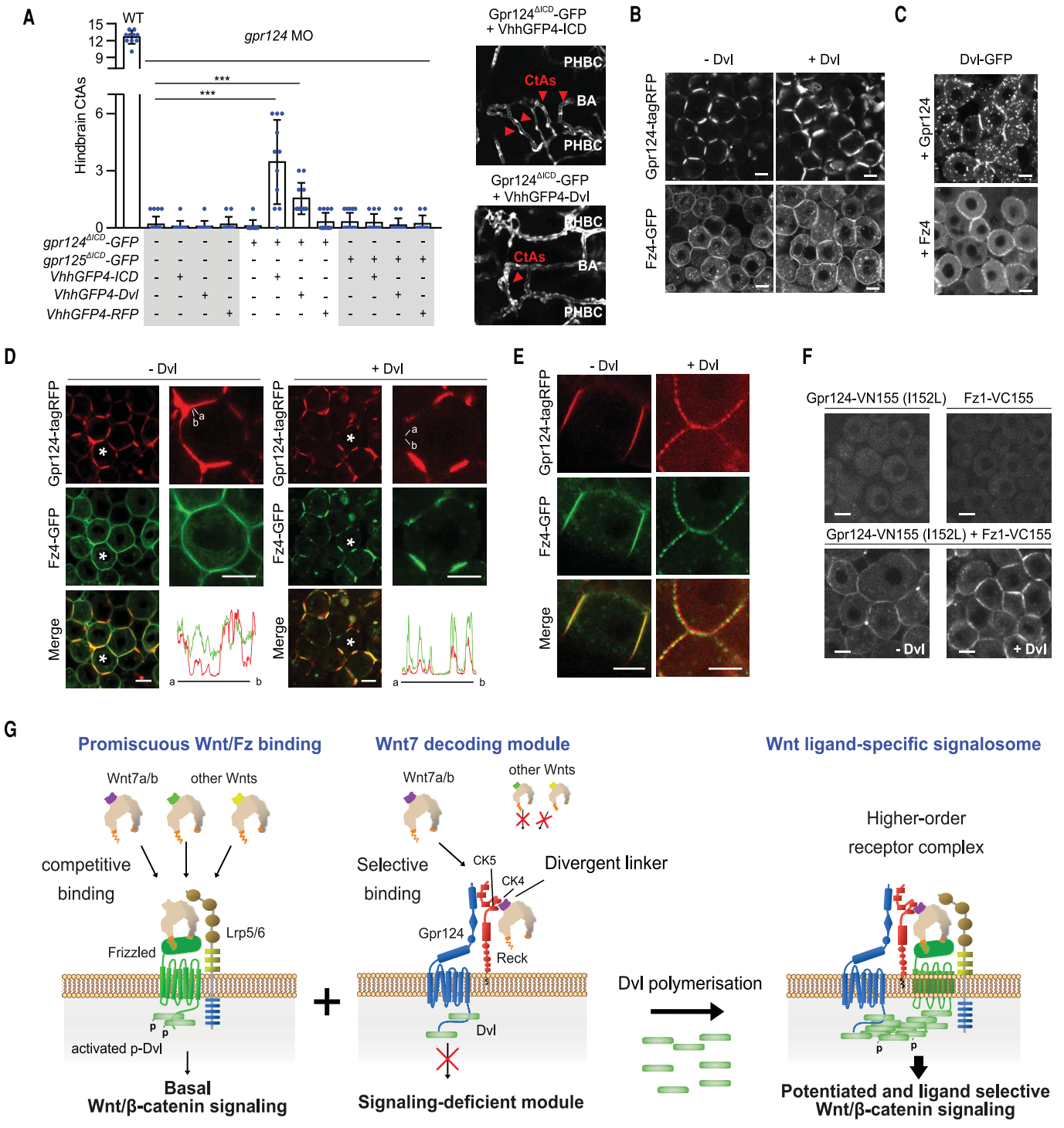

Fig. 6. Dvl polymers assemble ligand-specific Wnt signalosomes by linking Fz and Gpr124. (**A**) Hindbrain CtAs of WT or *gpr124* morphant embryos at 60 hours post fertilization, injected at the one-cell stage with 50 pg of the indicated mRNA. The injected doses of mRNA were reduced compared with Fig. 4H so as to avoid the developmental toxicity of *VhhGFP4-Dvl* mRNA injections. Representative hindbrain vasculature is shown on the right. (**B**) Intracellular distribution of Fz4-GFP and Gpr124-tagRFP expressed individually or in the presence of Dvl in zebrafish blastula DEL cells. (**C**) Intracellular distribution of Dvl-GFP coexpressed with Fz4 or Gpr124 in zebrafish blastula DEL cells. (**D**) Intracellular distribution of coexpressed Fz4-GFP and Gpr124-tagRFP in the absence or presence of Dvl in zebrafish blastula DEL cells. The cells annotated with an asterisk are magnified at right, and the pixel intensity of the green and red channels along a virtual clockwise path following the cell cortex from a to b is plotted below. (**E**) Same as (D) in EVL cells. (**F**) BiFC signals in zebrafish DEL cells expressing Gpr124-VN155 (I152L) and Fz1-VC155 in the presence or absence of Dvl overexpression. (**G**) Integrated model for Gpr124/Reck-dependent, Wnt7-specific Fz signaling. Scale bars, 10 μm. ***$P < 0.001$; data represent mean ± SD.

Embryos were obtained and raised under standard conditions in accordance with European and national ethical and animal welfare guidelines (protocol approval number: CEBEA-IBMM-2017-22:65). Staging was performed according to Kimmel *et al.* (*42*). The transgenic and mutant lines used in this study are *Tg(kdrl:EGFP)*^{s843} (*43*), *Tg(kdrl:HRAS-mCherry)*^{s896} (*44*) and *gpr124*^{s984} (*22*).

Morpholinos, RNA constructs, and microinjection

Splice-blocking morpholinos targeting *gpr124* (ACTGATATTGATTTAACTCACCACA) (*22*) were purchased from Gene Tools and injected at the one-cell stage at 2 ng. Synthetic mRNAs were transcribed from NotI linearized pCS2 using the mMessage mMachine SP6 Kit (Thermo Fisher Scientific) and injected into one-cell stage zebrafish embryos.

Somatic gene disruption in zebrafish by CRISPR/Cas9

The *gpr124*^{ICD}-targeting sgRNA*s* constructs (sgRNA 1-12) were obtained by in vitro annealing of the following primers (1-Fo: TAGGTGGCATGCTACAAAAAGC and 1-Rv: AAACGCTTTTTGTAGCATGCCA; 2-Fo: TAGGTTTGGGTCCGTAGGTGGA and 2-Rv: AAACTCCACCTACGGACCCAAA; 3-Fo: TAGGGTAATGGTTTGGGTCCGT and 3-Rv: AAACACGGACCCAAACCATTAC; 4-Fo: TAGGAGAAGAAGAGTAATGGTT and 4-Rv: AAACAACCATTACTCTTCTTCT; 5-Fo: TAGGAAGCTTGTAGTAGAACCA and 5-Rv: AAACTGGTTCTACTACAAGCTT; 6-Fo: TAGGCCATTCTGGCCCTCTGAA and 6-Rv: AAACTTCAGAGGGCCAGAATGG; 7-Fo: TAGGCCAACGGGCGGCACAGAG and 7-Rv: AAACCTCTGTGCCGCCCGTTGG; 8-Fo: TAGGGGCACAGAGGGGAAGGAC and 8-Rv: AAACGTCCTTCCCCTCTGTGCC; 9-Fo: TAGGTAGTGATGGAGGTAGCAG and 9-Rv: AAACCTGCTACCTCCATCACTA; 10-Fo: TAGGTGCCTTCGGTAGCACGTA and 10-Rv: AAACTACGTGCTACCGAAGGCA; 11-Fo: TAGGGGTATGAAGAGCAGGGTA and 11-Rv: AAACTACCCTGCTCTTCATACC; 12-Fo: TAGGTCGGTGGGTATGAAGAGC and 12-Rv: AAACGCTCTTCATACCCACCGA) and cloning into pT7-gRNA (Addgene #46759), as described in (*45*). sgRNA were transcribed from the BamHI linearized vector pT7-gRNA using the MEGAshortscript T7 kit (Thermo Fisher Scientific). The synthetic Cas9 mRNA was transcribed from the XbaI linearized vector pT3TS-nls-zCas9-nls (Addgene #46757) using the mMessage mMachine T3 Kit (Ambion). sgRNAs 1-12 (50 pg) and nls-zCas9-nls mRNA (150 pg) were injected into one-cell stage zebrafish embryos. The brain vasculature was analyzed and imaged at 48 hpf.

Whole-mount in situ hybridization (WISH)

Digoxigenin-labeled antisense riboprobes were synthesized with the digoxigenin (DIG) RNA labeling kit (Roche Diagnostics GmbH). Embryos were fixed in 4% paraformaldehyde overnight at 4°C and whole-mount in situ hybridization was performed using digoxigenin-labeled *myod1* riboprobes as previously described (*46*, *47*).

Expression plasmid constructs

Wnt, Frizzled, Reck and Gpr124 and their variants used in STF and PLA assays were expressed from the CMV promoter of the pCS2 plasmid except for the following plasmids: pRK5-Lrp5-rhotag, Fz4-GFP (Addgene #42197), Fz1 (Addgene #42253) and Fz5 (Addgene #42267), all kindly provided by J. Nathans. Single-point mutation variants, deletions and chimeras were generated using In-Fusion cloning (ST0345, Takara) and tandem overlapping PCR products. All constructs were confirmed by Sanger sequencing. Throughout this study, we used *Xenopus* Dvl-GFP (Addgene #16788, from the R. Moon laboratory), zebrafish Gpr124 and Gpr125 as well as mouse Reck and untagged Wnt ligands (*22*). The collection of active human Wnt-V5 ligands was kindly provided by the Xi He laboratory via Addgene (#43807 to #43825) (*48*). The activity of the V5-tagged ligands was verified by STF assays (fig. S22). Reck deletion variants correspond to the following amino acids of mouse Reck (NP_057887.2): Reck$^{\Delta CK1}$: 46-93; Reck$^{\Delta CK2}$: 113-150; Reck$^{\Delta CK3}$: 160-206; Reck$^{\Delta CK4}$: 225-272; Reck$^{\Delta CK5}$: 301-347; Reck$^{\Delta CK1\text{-}5}$: 46-347; Reck$^{\Delta CRD}$: 352-484 and Reck$^{\Delta KAZAL}$: 636-798. Gpr124 deletion variants correspond to the following amino acids of zebrafish Gpr124 (NP_001305000.1): Gpr124$^{\Delta ECD}$: 68-725 and Gpr124$^{\Delta TM2\text{-}7}$: 764-1030. The Gpr124 ICD used in deletion, swapping or fusion constructs corresponds to residues 1058-1367 of the full length protein (28-337 of the ICD), unless otherwise indicated. The ICD of Gpr124 is defined as the segment that follows the last transmembrane segment of the seven pass transmembrane protein as non-ambiguously defined by the InterPro server of EMBL-EBI (based on the Phobius transmembrane topology and signal peptide predictor from the Stockholm Bioinformatics Centre). The ICD of zebrafish Gpr125 (NP_001289153) and of zebrafish Fz2 (NP_571215.1) were similarly defined and correspond to the residues 1054-1346 and 526-550, respectively. Gpr124^{ECD}-TM^{CD27}-GFP was generated by replacing the 7-TM span of Gpr124 (residues 743-1030) by the TM of mouse CD27 (NP_001028298.1) (IFVTFSSMFLIFVLGAIL). The VhhGFP4-ICD construct was generated by fusing the Gpr124 ICD to the C terminus of VhhGFP4 [kindly provided by Markus Affolter (*28*)]. Gpr124$^{ICDFz2\Delta KTxxxW/\Delta ETTV}$ was generated by deleting the KTxxxW (KTLHSW) and ETTV motifs within the ICD of zebrafish Fz2. The BiFC constructs were subcloned from pBiFC-VC155 (Addgene #22011) and pBiFC-VN155 (I152L) (Addgene #27097). The HA tag was inserted after residue 22 in murine Reck, residue 47 in zebrafish Gpr124 and residue 22 in murine Fz5. The FLAG tag was inserted after residue 47 in zebrafish Gpr124. We thank the numerous colleagues that facilitated this work by depositing their plasmids at Addgene.

Cell culture and HEK293(T) mutant cell lines

HEK293T cells were obtained from ATCC (CRL-3216) and the HEK293 STF cell line was kindly provided by J. Nathans. WT and mutant cells were cultured in DMEM/F12 medium (Lonza) supplemented with 10% fetal bovine serum and maintained at 37°C in a humidified incubator equilibrated with 5% CO_2. *GPR124* and *RECK* were genetically inactivated using CRISPR/Cas9 approaches in HEK293-STF cells and *LRP5*, *LRP6* and *FZ* were inactivated in HEK293T cells. The mutant cell lines were obtained by the iterative CRISPR/Cas9-mediated mutagenesis strategy illustrated in Fig. 1A. CRISPR/Cas9 guide sequences were designed using the http://crispr.mit.edu website and were cloned into pSpCas9(BB)-2A-GFP (*49*). The top 1% of GFP$^+$ cells was isolated by FACS (AriaIII, BD Biosciences) 48 hours after transfection and distributed in 96-well plates for clonal expansion. In order to facilitate the genetic characterization of the mutant cell lines, clones generating multiple-peak derivative melt curves in high-resolution melt analyses were first counter-selected. For each gene, two independent PCR products flanking the target site (300-1000 bp PCR products centered on the PAM site) were gel purified and characterized by Sanger sequencing on both strands. The absence of WT alleles in the uncloned PCR product was verified and the number of different edited alleles (1, 2 or 3 in hypotriploid HEK293 cells) was deduced from the complexity of the chromatograms (fig. S1). For each gene, the two independent PCR products were then cloned in pCR™-Blunt II-TOPO® (Thermo Fisher Scientific) and individual colonies were sequenced until each edited allele was sequenced at least twice from each individual PCR amplicon. The number of analyzed colonies for the *FZ*$_{1\text{-}10}^{-/-}$ cell line is provided in table S1. The sequencing chromatograms form the identified individual clones were then aligned to ensure that the allelic complexity of the uncloned PCR can exhaustively be accounted for by the identified alleles (fig. S1). Finally, to exclude allelic exclusion by PCR amplification bias, the absence of WT alleles in the *FZ*$_{1\text{-}10}^{-/-}$ cell line was verified by whole exome sequencing.

STF dual luciferase assay

Cells were plated into 96-well plates and transfected after 24 hours in triplicate with Lipofectamine 2000 (Thermo Fisher Scientific). The amount of plasmid DNA transfected per well was optimized for each expression vector as follows: Renilla luciferase (0.5 ng), Wnt ligands (20 ng), Fz receptors (5 ng), Lrp5 (2.5 ng), Gpr124 (10 ng), Reck (5 ng) and Dkk-1 (10 ng) unless otherwise indicated. The total amount of DNA was adjusted to 100 ng per well with the empty pCS2 vector. Dual luciferase assays were performed using the STF cell line or by co-transfecting 20 ng of M50 Super 8x TOPFlash plasmid (Addgene #12456). Cells were harvested in passive lysis buffer (E1980, Promega) and the activities of the Firefly and Renilla luciferases were measured sequentially

using the Dual-Luciferase Reporter Assay system (E1980, Promega) 48 hours post transfection. The competition assays in Fig. 1G and fig. S5 were performed by plating cells as a 1:1:1 mixture at 90% confluency in 96-well plates 24 hours after transfection. Luciferase activity was measured 24 hours after co-culture. For siRNA, cells were plated into 96-well plates and transfected after 24 hours in triplicate using Lipofectamine 2000 (Thermo Fisher Scientific) with 1 pmol (per well) of *Dvl2* or control siRNAs (SASI_HS01_00104204 and SIC001, Sigma-Aldrich) together with the indicated plasmids.

Immunofluorescence and proximity ligation assay

Cells were grown in glass-coated chambers (IBIDI) and transfected after 24 hours with Lipofectamine 2000 (Thermo Fisher Scientific). Cells were fixed with 4% paraformaldehyde for 10 min at room temperature (RT) 48 hours post transfection. For immunofluorescence staining (IF), cells were blocked in 1% BSA-PBS for 30 min before being exposed to primary antibodies for 1 hour at RT. After three PBS washes, cells were incubated with secondary antibodies for 1 hour at RT. For anti-V5 staining of Wnt ligands, cells were additionally washed for 10 min in PBS 0.1% Tween 20 before incubation with the secondary antibody solution. For the proximity ligation assay (PLA) (Sigma-Aldrich), cells were blocked for 30 min at 37°C with the Blocking solution provided by the manufacturer before being incubated with the primary antibodies for 1 hour at RT. Cells were washed three times and incubated with the PLA probes anti-rabbit PLUS and anti-mouse MINUS for 1 hour at 37°C. After two PBS washes, cells were incubated with the Duolink Ligation solution for 30 min at 37°C. After two PBS washes, cells were incubated with the Duolink Amplification solution for 100 min at 37°C. The following antibodies were used: monoclonal mouse anti-V5 (R96025, Thermo Fisher Scientific) at 1:500 for IF and PLA, purified polyclonal rabbit anti-HA (H6908, Sigma-Aldrich) at 1:400 for IF and PLA and anti-mouse Alexa488-conjugated secondary antibody (Thermo Fisher Scientific) at 1:5000. Cells were stained for 2 min with Hoechst diluted to 10 $\mu g\ ml^{-1}$ in PBS.

Western blot, Dot blot, GST pull-down and coimmunoprecipitation

The following antibodies were used with an overnight incubation at 4°C: rabbit anti-DVL2 (1:1000, #3224S, Cell Signaling Technology), rabbit anti-DVL2-phospho T224 (1:1000, ab124941, Abcam), mouse monoclonal anti-V5 (1:1000, R96025, Thermo Fisher Scientific), mouse monoclonal anti-β-actin-peroxidase (1:50000, A3854, Sigma-Aldrich), chicken anti-GFP (1:5000, GFP-1010, Aves), and mouse monoclonal anti-FLAG M2 (1:1000, F1804, Sigma-Aldrich).

Dot blot analyses were performed according to manufacturer's protocol with a BioDot SF apparatus (Bio-Rad). Serial dilutions of supernatant were spotted onto a nitrocellulose membrane (GE Healthcare). After drying, the membrane was incubated with the antibodies as described above. For the coimmunoprecipitations assays, HEK293T were collected 48 hours after transfection from six-well plates and resuspended after two PBS washes in lysis buffer [150 mM NaCl, 25 mM Tris (pH 7.5) and 1% IGEPAL CA-630 (Sigma-Aldrich)] containing EDTA-free protease inhibitor cocktail (Roche) for 30 min at 4°C. After centrifugation at 20000 g for 10 min, the supernatant was incubated with 20 µl of anti-FLAG M2 affinity gel (A2220, Sigma-Aldrich) overnight at 4°C. Beads were washed five times with the lysis buffer and boiled in 2x Laemmli Sample buffer. For GST pull-downs, the coding sequence of Gpr124 ICD and its ΔETTV variant were fused downstream of GST sequences into pGEX-6P1 (GE Healthcare). The GST-fusion proteins were induced in *Escherichia coli* BL21 by exposure to 0.1 mM of IPTG in LB medium at 37°C for 4 hours. Cells were subsequently lysed in a cell disruptor (M110S, Microfluidics) and after centrifugation, the GST-fusion protein from the supernatant were immobilized on Glutathione Sepharose beads (17-0756-01, GE Healthcare). The Dvl-GFP and GFP constructs were transcripted using the mMESSAGE mMACHINE SP6 Transcription Kit (Thermo Fisher Scientific) and in vitro translated using the Rabbit Reticulocyte Lysate System provided by Promega (L4960) in the presence of S^{35}-methionine (NEG009T001MC, PerkinElmer). The beads were incubated with the radiolabeled proteins in PBS for 3 hours at 4°C with gentle mixing and then washed five times with cold PBS. The bound complex was resuspended in 2x Laemmli buffer, separated by SDS-page and analyzed by fluorography.

Microscopy and images processing

Cells and zebrafish embryos were imaged with a LSM710 confocal microscope and images were processed in ImageJ. Images of eye fusion phenotypes were taken on a Leica M165 FC. Brain vasculature renderings were generated using Imaris software (BitPlane).

The following method was used for the quantification of the PLA signal: The in situ PLA signals are seen as bright fluorescent dots of characteristic appearance. The signal lined the cell surface, as expected given the membrane localization of the receptors. For quantification, several images were acquired on LSM710 confocal microscope with a 20x objective. ImageJ was used to generate binary images by global thresholding and to determine the ratio of the total area occupied by the PLA-positive pixels to the DAPI-positive pixels, the latter being indicative of the number of cells in the field of view. The threshold values were manually adjusted to reflect the nuclear localization of DAPI and the focal membrane PLA signals. Identical threshold values were used for all images. On the dot plot, each dot represents the ratio of one image. Each image typically contained 50-100 cells.

Structural modeling

The structure of *Xenopus* Wnt8a (PDB ID: 4F0A) (*13*) was used as a starting model for Wnt7a. Missing residues and substitutions were modeled using the program Modeller (*50*). The modeling strategy included accounting for existing disulphide bridges as observed in XWnt8a. The initial best models were subjected to a conjugate-gradient energy minimization in vacuum with the Cα restrained and then freed in a second minimization step. These models were then embedded in a water box and electric neutrality was achieved by adding Na^+ counter ions at 150 mM. The whole system was again energy minimized in 3000 steps. The molecular dynamics simulation was carried out for 0.5 ns with the program NAMD 2.7 at constant temperature (310 K) and constant pressure (1 atm), with periodic boundaries and using CHARMM36 as force field (*51*). A time step of 2 fs was used to integrate the equations of motion. The short-range interactions were cut at 12 Å and the smooth-particle mesh Ewald method was used to calculate electrostatic interactions. Hydrogen atoms were constrained using the SHAKE algorithm. The resulting model is an average representation of the stable simulation.

Recombinant Reck-Fc fusions and synthetic peptides

The HA-tagged CK domain of Reck and its individual CK motif deletion variants were fused at the N terminus of the Fc region of human IgG1. The fusion vector was kindly provided by J. Nathans (*24*). Fc fusion proteins were recovered in serum-free FreeStyle 293 Expression Medium (Thermo Fisher Scientific) from the supernatant of HEK293T cell cultures 72 hours post transfection with Lipofectamine 2000 (Thermo Fisher Scientific). After collection, the supernatants were submitted to Protein G affinity purification (Protein G Sepharose 4 Fast Flow, Sigma-Aldrich). After acidic elution, protein purity was assessed by Coomassie Blue staining (Fig. 3A). Synthetic Wnt linker peptides were obtained from Chinapeptide Co., Ltd at purities of over 90%.

Isothermal titration calorimetry

ITC titrations were carried out on an Affinity ITC (TA Instruments). Prior to the measurement, Reck-CK-Fc and all Reck-CK-Fc fusions were dialyzed to Tris-NaCl buffer (50 mM Tris pH8, 300 mM NaCl). In each case Wnt-derived peptides were prepared with buffer from the last step of protein dialysis. The samples were filtered and degassed before being examined in the calorimeter and the titrations were performed at 25°C. All the experiments consisted of injection of constant volumes of 2 µL of titrant into the cell (200 µL) with a stirring rate of 75 rpm. Nominal sample concentrations were between 20 µM and 40 µM in the cell and 400 µM to 1.0 mM in the syringe. Actual sample concentrations were determined after dialysis or buffer exchange by measurement of their absorption at 280 nm or by the BCA method. All data were analyzed using the MicroCal Origin ITC 7.0 and NanoAnalyze software packages.

Atomic force microscopy

Glass coverslips coated with a thin gold layer were cleaned in an ultraviolet radiation and

ozone (UV-O) cleaner (Jetlight) for 15 min and subsequently immersed overnight in an ethanol solution containing 1 mM 16-mercaptododecahexanoic acid and 1-mercapto-1-undecanol at a 1:99 volumetric ratio. Substrates were then rinsed with ethanol, dried with N_2 and added to a solution containing equal volumes of 20 mg ml^{-1} *N*-hydroxysuccinimide (NHS) and 50 mg ml^{-1} 1-ethyl-3-(3-dimethylaminopropyl)-carbodiimide (EDC) for 30 min. The obtained NHS activated surfaces were rinsed with ultrapure water and incubated with 100 µl of a 10 µg ml^{-1} Protein G solution for 1 hour at RT. Samples were then washed with washing buffer (3 × 5 min) and further incubated with 100 µl blocking buffer for 1 hour at RT. Finally, 50 µl of a 0.2 µg ml^{-1} Reck-CK-Fc solution was added to the substrates for 1 hour, rinsed with washing buffer and subsequently used for AFM experiments. Single-molecule force spectroscopy (SMFS) measurements were performed in PBS buffer at RT using a Nanoscope VIII Multimode AFM (Bruker). Triangular AFM cantilevers (MSCT, Bruker) with silicon nitride tips and a nominal spring constant between 0.01-0.06 N m^{-1} were used. Cantilevers were calibrated at the end of each experiment using the thermal noise method (*52*). Functionalized tips were derivatized using a NHS-PEG_{27}-Malemide linker following a protocol described elsewhere (*53*) to covalently attach the Pep7b linking the cysteine residue added at the C terminus. After functionalization, the cantilevers were washed with PBS (3 × 5 min) and stored in individual wells of a multiwell dish containing 2 ml of PBS per well at 4°C until used in AFM experiments. Force-distance curves were recorded as 32x32 pixels arrays over 1 × 1 μm^2 areas, using an applied force of 250 pN, a contact time of 0.25 s and a constant approach and retraction speed of 1 µm s^{-1}. For dynamic force spectroscopy measurements, the retraction speed of the cantilever was varied as follows: 20 nm s^{-1}, 100 nm s^{-1}, 200 nm s^{-1}, 1 µm s^{-1}, 2 µm s^{-1}, 10 µm s^{-1} and 20 µm s^{-1}. Typically, at least 2000 force-distance curves were performed for each cantilever at a particular retraction speed. The collected data were analyzed using the Nanoscope Analysis software (Bruker). The retraction segment of each curve was analyzed and unbinding events were considered as specific if they occurred at a distance between 5-50 nm from the contact point. The minimum adhesion force was further used to calculate binding probabilities and build force distribution histograms. To reconstruct the energy landscape of the measured interactions, loading rates were calculated from the force vs time curve, as the slope of the adhesion event before the tip cantilever jumps off to surface. The dependency of the force with the loading rate was then plotted in dynamic force spectroscopy plots.

Statistical analysis

Statistical analysis was performed using GraphPad software. Data represent mean ± SD. p-values were calculated by the one-way ANOVA (post hoc Dunnett's test) and Student's *t* test for multiple and single comparisons of normally distributed data (STF and PLA assays) and by the Kruskal–Wallis (post hoc Dunn's test) for multiple comparisons of non-normally distributed data (CtA quantifications); $*P < 0.05$; $**P < 0.01$; $***P < 0.001$.

REFERENCES AND NOTES

1. C. Y. Logan, R. Nusse, The Wnt signaling pathway in development and disease. *Annu. Rev. Cell Dev. Biol.* **20**, 781–810 (2004). doi: 10.1146/annurev.cellbio.20.010403.113126; pmid: 15473860
2. R. Nusse, H. E. Varmus, Wnt genes. *Cell* **69**, 1073–1087 (1992). doi: 10.1016/0092-8674(92)90630-U; pmid: 1617723
3. P. Bhanot *et al*., A new member of the frizzled family from *Drosophila* functions as a Wingless receptor. *Nature* **382**, 225–230 (1996). doi: 10.1038/382225a0; pmid: 8717036
4. C. Niehrs, The complex world of WNT receptor signalling. *Nat. Rev. Mol. Cell Biol.* **13**, 767–779 (2012). doi: 10.1038/nrm3470; pmid: 23151663
5. B. T. MacDonald, X. He, Frizzled and LRP5/6 receptors for Wnt/β-catenin signaling. *Cold Spring Harb. Perspect. Biol.* **4**, a007880 (2012). doi: 10.1101/cshperspect.a007880; pmid: 23209147
6. J. C. Hsieh, A. Rattner, P. M. Smallwood, J. Nathans, Biochemical characterization of Wnt-frizzled interactions using a soluble, biologically active vertebrate Wnt protein. *Proc. Natl. Acad. Sci. U.S.A.* **96**, 3546–3551 (1999). doi: 10.1073/pnas.96.7.3546; pmid: 10097073
7. A. Kikuchi, H. Yamamoto, S. Kishida, Multiplicity of the interactions of Wnt proteins and their receptors. *Cell. Signal.* **19**, 659–671 (2007). doi: 10.1016/j.cellsig.2006.11.001; pmid: 17188462
8. C. H. Wu, R. Nusse, Ligand receptor interactions in the Wnt signaling pathway in *Drosophila*. *J. Biol. Chem.* **277**, 41762–41769 (2002). doi: 10.1074/jbc.M207850200; pmid: 12205098
9. E. J. Rulifson, C. H. Wu, R. Nusse, Pathway specificity by the bifunctional receptor frizzled is determined by affinity for wingless. *Mol. Cell* **6**, 117–126 (2000). doi: 10.1016/S1097-2765(05)00018-3; pmid: 10949033
10. S. L. Holmen, A. Salic, C. R. Zylstra, M. W. Kirschner, B. O. Williams, A novel set of Wnt-Frizzled fusion proteins identifies receptor components that activate β -catenin-dependent signaling. *J. Biol. Chem.* **277**, 34727–34735 (2002). doi: 10.1074/jbc.M204989200; pmid: 12121999
11. H. Yu, X. Ye, N. Guo, J. Nathans, Frizzled 2 and frizzled 7 function redundantly in convergent extension and closure of the ventricular septum and palate: Evidence for a network of interacting genes. *Development* **139**, 4383–4394 (2012). doi: 10.1242/dev.083352; pmid: 23095888
12. Y. K. Wang *et al*., A novel human homologue of the *Drosophila* frizzled wnt receptor gene binds wingless protein and is in the Williams syndrome deletion at 7q11.23. *Hum. Mol. Genet.* **6**, 465–472 (1997). doi: 10.1093/hmg/6.3.465; pmid: 9147651
13. C. Y. Janda, D. Waghray, A. M. Levin, C. Thomas, K. C. Garcia, Structural basis of Wnt recognition by Frizzled. *Science* **337**, 59–64 (2012). doi: 10.1126/science.1222879; pmid: 22653731
14. J. M. Stenman *et al*., Canonical Wnt signaling regulates organ-specific assembly and differentiation of CNS vasculature. *Science* **322**, 1247–1250 (2008). doi: 10.1126/science.1164594; pmid: 19023080
15. R. Daneman *et al*., Wnt/beta-catenin signaling is required for CNS, but not non-CNS, angiogenesis. *Proc. Natl. Acad. Sci. U.S.A.* **106**, 641–646 (2009). doi: 10.1073/pnas.0805165106; pmid: 19129494
16. S. Liebner *et al*., Wnt/β-catenin signaling controls development of the blood-brain barrier. *J. Cell Biol.* **183**, 409–417 (2008). doi: 10.1083/jcb.200806024; pmid: 18955553
17. M. Cullen *et al*., GPR124, an orphan G protein-coupled receptor, is required for CNS-specific vascularization and establishment of the blood-brain barrier. *Proc. Natl. Acad. Sci. U.S.A.* **108**, 5759–5764 (2011). doi: 10.1073/pnas.1017192108; pmid: 21421844
18. F. Kuhnert *et al*., Essential regulation of CNS angiogenesis by the orphan G protein-coupled receptor GPR124. *Science* **330**, 985–989 (2010). doi: 10.1126/science.1196554; pmid: 21071672
19. K. D. Anderson *et al*., Angiogenic sprouting into neural tissue requires Gpr124, an orphan G protein-coupled receptor. *Proc. Natl. Acad. Sci. U.S.A.* **108**, 2807–2812 (2011). doi: 10.1073/pnas.1019761108; pmid: 21282641
20. Y. Zhou, J. Nathans, Gpr124 controls CNS angiogenesis and blood-brain barrier integrity by promoting ligand-specific canonical wnt signaling. *Dev. Cell* **31**, 248–256 (2014). doi: 10.1016/j.devcel.2014.08.018; pmid: 25373781
21. E. Posokhova *et al*., GPR124 functions as a WNT7-specific coactivator of canonical β-catenin signaling. *Cell Reports* **10**, 123–130 (2015). doi: 10.1016/j.celrep.2014.12.020; pmid: 25558062
22. B. Vanhollebeke *et al*., Tip cell-specific requirement for an atypical Gpr124- and Reck-dependent Wnt/β-catenin pathway during brain angiogenesis. *eLife* **4**, 1–25 (2015). doi: 10.7554/eLife.06489; pmid: 26051822
23. F. Ulrich *et al*., Reck enables cerebrovascular development by promoting canonical Wnt signaling. *Development* **143**, 147–159 (2016). doi: 10.1242/dev.123059; pmid: 26657775
24. C. Cho, P. M. Smallwood, J. Nathans, Reck and Gpr124 Are Essential Receptor Cofactors for Wnt7a/Wnt7b-specific signaling in mammalian CNS angiogenesis and blood-brain barrier regulation. *Neuron* **95**, 1056–1073.e5 (2017). doi: 10.1016/j.neuron.2017.07.031; pmid: 28803732
25. P. E. Wright, H. J. Dyson, Intrinsically disordered proteins in cellular signalling and regulation. *Nat. Rev. Mol. Cell Biol.* **16**, 18–29 (2015). doi: 10.1038/nrm3920; pmid: 25531225
26. M. L. H. Chu *et al*., structural Studies of Wnts and identification of an LRP6 binding site. *Structure* **21**, 1235–1242 (2013). doi: 10.1016/j.str.2013.05.006; pmid: 23791946
27. N. Bostaille, A. Gauquier, L. Twyffels, B. Vanhollebeke, Molecular insights into Adgra2/Gpr124 and Reck intracellular trafficking. *Biol. Open* **5**, 1874–1881 (2016). doi: 10.1242/bio.021287; pmid: 27979830
28. S. Harmansa, I. Alborelli, D. Bieli, E. Caussinus, M. Affolter, A nanobody-based toolset to investigate the role of protein localization and dispersal in *Drosophila*. *eLife* **6**, 1–22 (2017). doi: 10.7554/eLife.22549; pmid: 28395731
29. X. Li *et al*., Gpr125 modulates Dishevelled distribution and planar cell polarity signaling. *Development* **140**, 3028–3039 (2013). doi: 10.1242/dev.094839; pmid: 23821037
30. S. Yanagawa, F. van Leeuwen, A. Wodarz, J. Klingensmith, R. Nusse, The Dishevelled protein is modified by wingless signaling in *Drosophila*. *Genes Dev.* **9**, 1087–1097 (1995). doi: 10.1101/gad.9.9.1087; pmid: 7744250
31. X. Huang *et al*., Phosphorylation of Dishevelled by protein kinase RIPK4 regulates Wnt signaling. *Science* **339**, 1441–1445 (2013). doi: 10.1126/science.1232253; pmid: 23371553
32. M. Gammons, M. Bienz, Multiprotein complexes governing Wnt signal transduction. *Curr. Opin. Cell Biol.* **51**, 42–49 (2018). doi: 10.1016/j.ceb.2017.10.008; pmid: 29153704
33. M. Bienz, Signalosome assembly by domains undergoing dynamic head-to-tail polymerization. *Trends Biochem. Sci.* **39**, 487–495 (2014). doi: 10.1016/j.tibs.2014.08.006; pmid: 25239056
34. J. Bilic *et al*., Wnt induces LRP6 signalosomes and promotes dishevelled-dependent LRP6 phosphorylation. *Science* **316**, 1619–1622 (2007). doi: 10.1126/science.1137065; pmid: 17569865
35. M. V. Gammons, M. Renko, C. M. Johnson, T. J. Rutherford, M. Bienz, Wnt signalosome assembly by DEP domain swapping of Dishevelled. *Mol. Cell* **64**, 92–104 (2016). doi: 10.1016/j.molcel.2016.08.026; pmid: 27692984
36. M. B. Lai *et al*., TSPAN12 is a Norrin Co-receptor that amplifies Frizzled4 ligand selectivity and signaling. *Cell Reports* **19**, 2809–2822 (2017). doi: 10.1016/j.celrep.2017.06.004; pmid: 28658627
37. Z. F. Zimmerman, R. T. Moon, A. J. Chien, Targeting Wnt pathways in disease. *Cold Spring Harb. Perspect. Biol.* **4**, a008086 (2012). doi: 10.1101/cshperspect.a008086; pmid: 23001988
38. A. Koval, V. L. Katanaev, Platforms for high-throughput screening of Wnt/Frizzled antagonists. *Drug Discov. Today* **17**, 1316–1322 (2012). doi: 10.1016/j.drudis.2012.07.007; pmid: 22819927
39. H. Clevers, R. Nusse, Wnt/β-catenin signaling and disease. *Cell* **149**, 1192–1205 (2012). doi: 10.1016/j.cell.2012.05.012; pmid: 22682243
40. E. Driehuis, H. Clevers, WNT signalling events near the cell membrane and their pharmacological targeting for the treatment of cancer. *Br. J. Pharmacol.* **174**, 4547–4563 (2017). doi: 10.1111/bph.13758; pmid: 28244067
41. J. Chang *et al*., Gpr124 is essential for blood-brain barrier integrity in central nervous system disease. *Nat. Med.* **23**, 450–460 (2017). doi: 10.1038/nm.4309; pmid: 28288111
42. C. B. Kimmel, W. W. Ballard, S. R. Kimmel, B. Ullmann, T. F. Schilling, Stages of embryonic development of the

zebrafish. *Dev. Dyn.* **203**, 253–310 (1995). doi: 10.1002/aja.1002030302; pmid: 8589427
43. S. W. Jin, D. Beis, T. Mitchell, J. N. Chen, D. Y. R. Stainier, Cellular and molecular analyses of vascular tube and lumen formation in zebrafish. *Development* **132**, 5199–5209 (2005). doi: 10.1242/dev.02087; pmid: 16251212
44. N. C. Chi *et al*., Foxn4 directly regulates tbx2b expression and atrioventricular canal formation. *Genes Dev.* **22**, 734–739 (2008). doi: 10.1101/gad.1629408; pmid: 18347092
45. L. E. Jao, S. R. Wente, W. Chen, Efficient multiplex biallelic zebrafish genome editing using a CRISPR nuclease system. *Proc. Natl. Acad. Sci. U.S.A.* **110**, 13904–13909 (2013). doi: 10.1073/pnas.1308335110; pmid: 23918387
46. E. S. Weinberg *et al*., Developmental regulation of zebrafish MyoD in wild-type, no tail and spadetail embryos. *Development* **122**, 271–280 (1996). pmid: 8565839
47. C. Thisse, B. Thisse, High-resolution in situ hybridization to whole-mount zebrafish embryos. *Nat. Protoc.* **3**, 59–69 (2008). doi: 10.1038/nprot.2007.514; pmid: 18193022
48. B. T. MacDonald *et al*., Disulfide bond requirements for active Wnt ligands. *J. Biol. Chem.* **289**, 18122–18136 (2014). doi: 10.1074/jbc.M114.575027; pmid: 24841207
49. F. A. Ran *et al*., Genome engineering using the CRISPR-Cas9 system. *Nat. Protoc.* **8**, 2281–2308 (2013). doi: 10.1038/nprot.2013.143; pmid: 24157548
50. B. Webb, A. Sali, *Current Protocols in Bioinformatics* (John Wiley & Sons, 2016), vol. 54, p. 5.6.1-5.6.37.
51. J. C. Phillips *et al*., Scalable molecular dynamics with NAMD. *J. Comput. Chem.* **26**, 1781–1802 (2005). doi: 10.1002/jcc.20289; pmid: 16222654
52. H. J. Butt, M. Jaschke, Calculation of thermal noise in atomic force microscopy. *Nanotechnology* **6**, 1–7 (1995). doi: 10.1088/0957-4484/6/1/001
53. L. Wildling *et al*., Probing binding pocket of serotonin transporter by single molecular force spectroscopy on living cells. *J. Biol. Chem.* **287**, 105–113 (2012). doi: 10.1074/jbc.M111.304873; pmid: 22033932
54. R. W. Friddle, A. Noy, J. J. De Yoreo, Interpreting the widespread nonlinear force spectra of intermolecular bonds. *Proc. Natl. Acad. Sci. U.S.A.* **109**, 13573–13578 (2012). doi: 10.1073/pnas.1202946109; pmid: 22869712

ACKNOWLEDGMENTS

We thank J. Nathans (Johns Hopkins), R. Nusse (Stanford), and V. L. Katanaev (UNIL) for advice and fruitful discussions. We thank E. Dupont, S. Rosar, J. Marchal, V. Micha, S. Denanglaire, J. Declercq, L. Sanderson, M. Boeckstaens, N. De Henau, and L. Twyffels (ULB) for their help. **Funding:** M.E. and N.B. are FRIA fellows from Fonds de la Recherche Scientifique–FNRS. P.C. and D.A. are a postdoctoral researcher and research associate of the FRS.-FNRS, respectively. Work in the B.V. laboratory is supported by FNRS (MIS F.4543.15), the Concerted Research Action (ARC), the Fondation ULB, the Queen Elisabeth Medical Foundation (Q.E.M.F.), and FRFS-WELBIO (CR-2017S-05). CMMI is supported by the European Regional Development Fund and the Walloon Region. **Author contributions:** All authors performed research and/or analyzed data. All authors discussed results and edited the manuscript. B.V. designed the research and wrote the manuscript. **Competing interests:** The ULB (B.V.) has filed a patent on the neurological applications of the Gpr124/Reck-mediated signaling mechanism. **Data and materials availability:** All data are available in the main text or the supplementary materials. Correspondence and requests for materials should be addressed to B.V.

SUPPLEMENTARY MATERIALS

www.sciencemag.org/content/361/6403/eaat1178/suppl/DC1
Figs. S1 to S22
Table S1

30 January 2018; accepted 26 June 2018
Published online 19 July 2018
10.1126/science.aat1178

Science

A molecular mechanism for Wnt ligand-specific signaling

Marie Eubelen, Naguissa Bostaille, Pauline Cabochette, Anne Gauquier, Patricia Tebabi, Andra C. Dumitru, Melanie Koehler, Philipp Gut, David Alsteens, Didier Y. R. Stainier, Abel Garcia-Pino and Benoit Vanhollebeke

Science **361** (6403), eaat1178.
DOI: 10.1126/science.aat1178originally published online July 19, 2018

How Wnt ligands achieve specificity

Wnt signaling is essential for development, tissue homeostasis, and disease. The 19 members of the Wnt family interact promiscuously with the 10 Frizzled receptors, raising the question of how ligand-specific discrimination is achieved in a biological context. Eubelen *et al.* used experiments in zebrafish to show that cells are equipped with decoding modules that bind Wnt with high specificity and trigger signal amplification via their recruitment into higher-order Frizzled signalosomes (see the Perspective by Kim and Goentoro). Thus, distinct Wnt ligand-receptor pairs can be targeted specifically for therapeutic purposes.

Science, this issue p. eaat1178; see also p. 643